# Online appendix

# A Additional summary statistics

In this section, we provide further details on the construction of the stable lights or radiance-calibrated data and compare their characteristics.

The main advantage of the stable lights series is that they are available as an annual panel from 1992 until 2013. Moreover, for several years more than one satellite orbited Earth, resulting in a total of 34 satellite years. The radiance-calibrated data, by contrast, are based on rare flights of satellites that were about to be decommissioned and could be operated with a different gain setting (lower or higher amplification settings). These auxiliary data are only available for seven years over the entire period from 1996 to 2010. NOAA blends the stable lights data from normal flight operations with these data to obtain the radiance-calibrated series (Elvidge et al., 1999, Ziskin et al., 2010, Hsu et al., 2015). The resulting night light intensities are free of top-coding and have no theoretical upper bound.

Several technical issues and measurement errors, occurring when the different fixed gain images are merged at NOAA, produce a lot of variability in the radiance-calibrated data: *i)* the low amplification data are based on considerably fewer orbits than the stable lights series (often covering only small parts of a year), *ii)* they are generated by blending different parts of the frequency spectrum which are deemed reliable, *iii)* higher light intensities are supported by fewer and fewer fixed-gain images[1], and *iv)* fires or stray lights are not fully removed from the auxiliary data. All this contributes to the high variance across different radiance-calibrated satellite-years.[2] Because of this instability, together with the fact that they are only available for seven out of 22 years, we only rely on the radiance-calibrated data to infer the shape of the distribution at the top. The relative ranks of pixels are consistently measured across the different satellites and less prone to be affected by measurement errors.

Table A-1 reports summary statistics for the 34 stable light satellite years and the seven radiance-calibrated years. Between 2.7% and 5.9% of all pixels in the stable lights images reach the top of the scale (i.e., 55 DN to 63 DN), more so in later years. As the radiance-calibrated lights do not suffer from top-coding, their mean, standard deviation, and Gini in lights are much higher. Rather than being capped at 63 DN, they reach maximum values from 2000 to 5000 DN. The fluctuations across satellites are reflected in the overall mean light intensity but are most apparent at the top. The maximum

[1]Consider the 2010 radiance-calibrated product. The maximum number of cloud-free images is 134, the suburbs of Paris are informed by about 50–60 cloud-free images, but the city core only by 10–20 images. This pattern repeats itself throughout all major cities.

[2]Measurement errors are also present in the stable lights data and affect their reliability in the time-series dimension but to a much lesser extent. The sensors of the satellites deteriorated over their lifetime and had to be replaced every couple of years, which implies that later recordings of any particular satellite tend to be the brightest (although this is not a hard rule). In panel regressions, economists usually resort to a combination of satellite and time fixed effects to partially address this issue.

light intensity doubles within three years and then decreases again by a similar amount (whereas the mean increases and decreases by about 27% over the same period).

Table A-2 confirms that these fluctuations are not driven by a few outliers. Instead of examining overall maxima, we now report various percentiles for the seven satellite-years of radiance-calibrated data and the means above these percentiles. For example, the top 2% begin at 147.01 DN in the 1996 data, at 214.59 DN in 2003, and again at 150.90 DN in 2010. The means above the various percentiles also vary over time. The differences are largest in absolute values at the very top but remain sizable throughout the distribution. We attribute this variation to the fact that fewer and fewer daily images inform the top of the distribution.

Table A-3 illustrates that not all differences between the stable lights and radiance-calibrated data can be attributed to top-coding. It regresses all pixels below 55 DN of the stable lights on the radiance-calibrated lights, where top-coding is supposed to not play a role. We find a regression coefficient around one-half rather than equivalence. This absence of a one-to-one correspondence is owed to the lack of onboard calibration, blooming (Abrahams et al., 2018), the presence of stray light (Hsu et al., 2015), and geo-location errors (Tuttle et al., 2013).

Table A-4 shows the maximum values attained by the seven satellite-years of radiance-calibrated data in 30 selected cities. Despite considerable variability over time, the relative ranking is in line with our expectations. The light intensity of the brightest pixel in New York City, for example, is about ten times greater than that of the brightest pixel in Nairobi. Note that the average maximum light intensity hardly exceeds 2000 DN, no matter if we compute it for London, New York, or Shanghai. This is why we restrict the maximum light intensities generated by our pixel-level correction to 2000 DN. Alternatively, our approach can be interpreted as fixing the radiance-calibrated scale at its 2010 or 2000 range, as these are the two years in which no city pixel exceeds 2000 DN.

Table A-5 reports the maximum light intensities recorded within 25 kilometers of the city center in 988 world cities with more than 500,000 inhabitants. Table A-6 adds the rank-correlations. The latter are much higher and typically around 0.90–0.95 for adjacent radiance-calibrated years, which supports our preference for pixel ranks over their actual values.

**Table A-1** – Summary statistics of the stable lights and radiance-calibrated data

| | *Stable lights* | | | | | *Radiance-calibrated* | | | |
|---|---|---|---|---|---|---|---|---|---|
| Year | Flight No. | Mean | Std. Dev. | Gini | % ≥ 55 | Mean | Std. Dev. | Gini | Max |
| 1992 | F10 | 13.83 | 13.51 | 0.44 | 3.81 | | | | |
| 1993 | F10 | 11.96 | 12.81 | 0.46 | 3.12 | | | | |
| 1994 | F10 | 12.02 | 13.31 | 0.48 | 3.49 | | | | |
| | F12 | 14.65 | 13.93 | 0.44 | 4.20 | | | | |
| 1995 | F12 | 13.09 | 13.57 | 0.46 | 3.76 | | | | |
| 1996 | F12 | 12.69 | 13.36 | 0.46 | 3.51 | 19.42 | 55.63 | 0.65 | 2064 |
| 1997 | F12 | 13.45 | 13.74 | 0.45 | 3.94 | | | | |
| | F14 | 10.98 | 12.87 | 0.49 | 3.16 | | | | |
| 1998 | F12 | 13.89 | 13.89 | 0.45 | 4.18 | | | | |
| | F14 | 10.94 | 12.78 | 0.49 | 3.05 | | | | |
| 1999 | F12 | 14.74 | 14.34 | 0.44 | 4.67 | 19.53 | 56.93 | 0.64 | 4698 |
| | F14 | 10.15 | 12.31 | 0.49 | 2.78 | | | | |
| 2000 | F14 | 11.34 | 12.99 | 0.49 | 3.18 | 22.88 | 65.84 | 0.63 | 5552 |
| | F15 | 13.25 | 13.34 | 0.44 | 3.70 | | | | |
| 2001 | F14 | 11.64 | 13.32 | 0.49 | 3.50 | | | | |
| | F15 | 12.93 | 13.26 | 0.45 | 3.54 | | | | |
| 2002 | F14 | 12.14 | 13.70 | 0.49 | 3.77 | | | | |
| | F15 | 13.18 | 13.44 | 0.45 | 3.72 | | | | |
| 2003 | F14 | 11.96 | 13.72 | 0.49 | 3.82 | 24.83 | 67.57 | 0.65 | 4186 |
| | F15 | 10.28 | 12.45 | 0.50 | 2.70 | | | | |
| 2004 | F15 | 10.08 | 12.52 | 0.51 | 2.76 | 24.07 | 65.94 | 0.66 | 4357 |
| | F16 | 11.82 | 13.04 | 0.46 | 3.40 | | | | |
| 2005 | F15 | 10.44 | 12.73 | 0.51 | 2.79 | | | | |
| | F16 | 10.44 | 12.54 | 0.49 | 2.85 | | | | |
| 2006 | F15 | 10.56 | 12.91 | 0.51 | 2.93 | 20.63 | 50.93 | 0.63 | 3333 |
| | F16 | 12.26 | 13.37 | 0.47 | 3.48 | | | | |
| 2007 | F15 | 10.74 | 12.82 | 0.50 | 2.79 | | | | |
| | F16 | 13.05 | 13.79 | 0.46 | 4.03 | | | | |
| 2008 | F16 | 12.97 | 13.84 | 0.47 | 3.95 | | | | |
| 2009 | F16 | 13.50 | 14.12 | 0.47 | 4.17 | | | | |
| 2010 | F18 | 17.55 | 15.35 | 0.43 | 5.91 | 19.04 | 44.35 | 0.60 | 2110 |
| 2011 | F18 | 14.78 | 14.68 | 0.46 | 4.94 | | | | |
| 2012 | F18 | 16.44 | 15.20 | 0.44 | 5.76 | | | | |
| 2013 | F18 | 16.23 | 15.20 | 0.44 | 5.78 | | | | |

*Notes*: The table reports summary statistics using a 10% sample of the stable lights and radiance-calibrated data at the pixel level, where each pixel is 30 × 30 arc seconds. There are several years when two DMSP satellites were concurrently recording data for the stable lights series, so that there are 34 satellite-years between 1992 and 2013. The radiance-calibrated data are only available for the following periods: 16 Mar 96 – 12 Feb 97 (1996), 19 Jan 99 – 11 Dec 99 (1999), 03 Jan 00 – 29 Dec 00 (2000), 30 Dec 02 – 11 Nov 2003 (2003), 18 Jan 04 – 16 Dec 04 (2004), 28 Nov 05 – 24 Dec 06 (2006), and 11 Jan 10 – 9 Dec 10 (2010), although the actual coverage in terms of days often refers to a much smaller period.

**Table A-2** – Summary statistics of the radiance-calibrated data (top shares)

| Year | 1996 | 1999 | 2000 | 2003 | 2004 | 2006 | 2010 |
|---|---|---|---|---|---|---|---|
| | *Panel a) Top 5%* | | | | | | |
| Percentile ($x$) | 62.87 | 66.74 | 73.75 | 94.60 | 90.97 | 74.97 | 64.84 |
| Mean above $x$ | 186.04 | 197.42 | 228.61 | 245.59 | 236.80 | 189.34 | 166.90 |
| | *Panel b) Top 4%* | | | | | | |
| Percentile ($x$) | 76.30 | 84.79 | 95.62 | 119.27 | 114.26 | 94.03 | 81.98 |
| Mean above $x$ | 215.29 | 228.01 | 264.84 | 280.40 | 270.51 | 215.70 | 190.42 |
| | *Panel c) Top 3%* | | | | | | |
| Percentile ($x$) | 98.42 | 114.12 | 131.13 | 154.40 | 149.82 | 122.72 | 108.27 |
| Mean above $x$ | 258.23 | 271.33 | 315.97 | 328.70 | 317.06 | 251.82 | 222.49 |
| | *Panel d) Top 2%* | | | | | | |
| Percentile ($x$) | 147.01 | 166.33 | 198.77 | 214.59 | 207.97 | 168.84 | 150.90 |
| Mean above $x$ | 327.60 | 338.23 | 393.22 | 402.32 | 387.54 | 305.83 | 269.84 |
| | *Panel e) Top 1%* | | | | | | |
| Percentile ($x$) | 259.04 | 275.41 | 318.53 | 331.88 | 314.53 | 255.44 | 229.79 |
| Mean above $x$ | 460.17 | 463.60 | 534.81 | 538.85 | 519.98 | 404.80 | 354.36 |
| | *Panel f) Top 0.1%* | | | | | | |
| Percentile ($x$) | 729.41 | 716.94 | 815.16 | 822.00 | 805.43 | 605.13 | 511.62 |
| Mean above $x$ | 979.91 | 960.86 | 1117.96 | 1110.62 | 1111.93 | 806.63 | 687.53 |
| | *Panel g) Top 0.01%* | | | | | | |
| Percentile ($x$) | 1355.38 | 1279.48 | 1528.71 | 1491.25 | 1516.16 | 1085.71 | 936.22 |
| Mean above $x$ | 1551.16 | 1652.31 | 1893.03 | 1828.03 | 1914.32 | 1316.93 | 1137.76 |

*Notes*: The table shows summary statistics of the radiance-calibrated data at the various percentiles. The input data are a 10% representative sample of all non-zero lights in the radiance-calibrated data above the defined threshold at the pixel level, where each pixel is $30 \times 30$ arc seconds.

**Table A-3** – Regression of stable lights on radiance-calibrated data

| Year | 1996 | 1999 | 2000 | 2003 | 2004 | 2006 | 2010 |
|---|---|---|---|---|---|---|---|
| Stable lights | 0.5557 | 0.5502 | 0.4241 | 0.4357 | 0.3473 | 0.4874 | 0.7468 |
| | (0.0002) | (0.0003) | (0.0002) | (0.0002) | (0.0001) | (0.0002) | (0.0004) |
| Constant | 4.6422 | 5.5218 | 3.9172 | 3.6007 | 3.2069 | 2.9392 | 6.4094 |
| | (0.0045) | (0.0054) | (0.0044) | (0.0043) | (0.0036) | (0.0037) | (0.0066) |
| $R^2$ | 0.7440 | 0.7013 | 0.7115 | 0.7709 | 0.7873 | 0.8011 | 0.6319 |

*Notes*: The table reports OLS estimates of a regression of all pixels smaller than 55 DN of the stable lights on their radiance-calibrated counterpart in all those years for which both data sources are available. Standard errors are in parentheses. The data are a 10% random sample of lights at the pixel level, where each pixel is $30 \times 30$ arc seconds.

**Table A-4** – Maximum light intensities in 30 selected cities over time

| City | 1996 | 1999 | 2000 | 2003 | 2004 | 2006 | 2010 | Average |
|---|---|---|---|---|---|---|---|---|
| Beijing | 977.94 | 2265.07 | 3160.86 | 2911.25 | 2979.75 | 1575.00 | 1262.30 | 2161.74 |
| Berlin | 393.16 | 904.28 | 648.10 | 883.65 | 1045.85 | 474.82 | 357.46 | 672.48 |
| Bogota | 416.75 | 661.73 | 774.02 | 828.82 | 602.80 | 622.18 | 489.89 | 628.02 |
| Brussels | 882.44 | 1026.01 | 1410.89 | 840.66 | 935.03 | 920.00 | 465.11 | 925.73 |
| Cairo | 1785.16 | 1709.40 | 1768.79 | 2013.90 | 1876.90 | 1273.33 | 940.31 | 1623.97 |
| Calgary | 1669.85 | 1084.76 | 2077.92 | 1520.70 | 822.00 | 731.15 | 721.22 | 1232.51 |
| Casablanca | 729.69 | 919.44 | 769.98 | 1075.77 | 1214.73 | 708.33 | 620.97 | 862.70 |
| Damascus | 952.80 | 1302.40 | 921.07 | 862.37 | 1068.60 | 852.94 | 766.55 | 960.96 |
| Dhaka | 321.94 | 427.63 | 370.72 | 458.76 | 438.15 | 296.59 | 208.28 | 360.29 |
| Dubai | 1882.37 | 2137.78 | 2144.43 | 2068.70 | 2104.32 | 1457.14 | 1169.82 | 1852.08 |
| Edinburgh | 453.18 | 811.04 | 537.69 | 767.20 | 973.48 | 425.24 | 518.75 | 640.94 |
| Foshan | 537.46 | 715.98 | 1410.36 | 1625.73 | 1499.66 | 1142.86 | 1164.98 | 1156.72 |
| Istanbul | 379.97 | 1018.80 | 779.05 | 681.09 | 902.42 | 652.94 | 743.44 | 736.82 |
| Jakarta | 1100.27 | 683.82 | 664.56 | 788.43 | 1381.62 | 805.95 | 632.81 | 865.35 |
| Johannesburg | 517.62 | 672.89 | 712.18 | 688.42 | 729.53 | 528.57 | 448.43 | 613.95 |
| London | 984.36 | 2332.85 | 1940.67 | 1664.98 | 1356.30 | 1111.11 | 511.40 | 1414.52 |
| Los Angeles | 1214.68 | 1331.26 | 1805.43 | 1661.61 | 1561.80 | 1153.33 | 1199.81 | 1418.27 |
| Manila | 629.67 | 629.42 | 695.65 | 810.81 | 808.30 | 580.00 | 513.82 | 666.81 |
| Moscow | 976.78 | 1202.94 | 1496.44 | 1729.90 | 2383.80 | 1250.00 | 1285.51 | 1475.05 |
| Mosul | 136.55 | 139.61 | 161.64 | 194.56 | 244.10 | 85.71 | 148.04 | 158.60 |
| Mumbai | 527.60 | 543.47 | 622.09 | 753.50 | 730.67 | 550.00 | 414.87 | 591.74 |
| Nairobi | 211.83 | 180.27 | 188.66 | 191.45 | 173.54 | 174.02 | 164.13 | 183.41 |
| New York | 1664.97 | 3342.95 | 2145.71 | 2123.50 | 1575.50 | 1815.38 | 1366.45 | 2004.92 |
| Paris | 1177.72 | 1827.80 | 2444.32 | 1794.70 | 1430.28 | 1425.00 | 874.55 | 1567.77 |
| Rio de Janeiro | 748.92 | 926.51 | 917.27 | 708.83 | 699.31 | 484.08 | 461.57 | 706.64 |
| Seoul | 1327.49 | 1847.79 | 1999.46 | 2049.13 | 2285.16 | 1735.71 | 924.85 | 1738.51 |
| Shanghai | 1123.89 | 1965.24 | 1906.01 | 3982.13 | 2931.80 | 2307.14 | 1926.59 | 2306.12 |
| Sydney | 1070.85 | 1138.12 | 954.50 | 1223.82 | 1262.36 | 840.00 | 513.78 | 1000.49 |
| Tel Aviv | 997.83 | 1284.19 | 1679.72 | 1446.72 | 1397.40 | 1188.24 | 1099.83 | 1299.13 |
| Tokyo | 1515.98 | 1456.54 | 1790.01 | 1963.82 | 1775.52 | 1322.22 | 1842.57 | 1666.67 |

*Notes:* The table report the maximum light intensity in DN recorded within 25 km radius of the city center in a selection of cities. The input data are the radiance-calibrated lights. City locations are obtained from the Natural Earth point data of major populated places.

**Table A-5** – Correlation matrix of maximum city lights

| Years | 1996 | 1999 | 2000 | 2003 | 2004 | 2006 | 2010 |
|---|---|---|---|---|---|---|---|
| 1996 | 1.0000 | | | | | | |
| 1999 | 0.8612 | 1.0000 | | | | | |
| 2000 | 0.8551 | 0.9134 | 1.0000 | | | | |
| 2003 | 0.8065 | 0.8733 | 0.8990 | 1.0000 | | | |
| 2004 | 0.7713 | 0.8587 | 0.8601 | 0.9176 | 1.0000 | | |
| 2006 | 0.8106 | 0.8741 | 0.8953 | 0.9379 | 0.9305 | 1.0000 | |
| 2010 | 0.7406 | 0.7806 | 0.7839 | 0.8501 | 0.8513 | 0.8939 | 1.0000 |

*Notes*: The table reports correlations between the maximum light intensities recorded within 25 km radius of the city center of 988 world cities with more than 500,000 inhabitants.

**Table A-6** – Rank correlation matrix of maximum city lights

| Years | 1996 | 1999 | 2000 | 2003 | 2004 | 2006 | 2010 |
|---|---|---|---|---|---|---|---|
| 1996 | 1.0000 | | | | | | |
| 1999 | 0.9161 | 1.0000 | | | | | |
| 2000 | 0.9126 | 0.9557 | 1.0000 | | | | |
| 2003 | 0.8448 | 0.9129 | 0.9328 | 1.0000 | | | |
| 2004 | 0.8453 | 0.9048 | 0.9162 | 0.9542 | 1.0000 | | |
| 2006 | 0.8621 | 0.9066 | 0.9253 | 0.9548 | 0.9491 | 1.0000 | |
| 2010 | 0.8096 | 0.8489 | 0.8645 | 0.8970 | 0.8968 | 0.9270 | 1.0000 |

*Notes*: The table reports rank correlations between the maximum light intensities recorded within 25 km radius of the city center of 988 world cities with more than 500,000 inhabitants.

# B The top-coding threshold

The influence of top-coding in the DMSP-OLS satellite data has been underestimated in part because much of the literature assumes it only affects pixels with the highest recorded value. However, even though the scale of stable lights goes up to 63, we have good reason to assume that many pixels with DNs of 62, 61, down to the mid-50s, are subject to top-coding and should be brighter than they are recorded in the data.

The rationale behind this conjecture is straightforward. The stable lights data were already averaged at least twice during the data construction. First, the DMSP satellites averaged several higher resolution pixels on-board to reduce the amount of information that needs to be transmitted down to Earth. The OLS system recorded images at a nominal resolution of 0.56 km, which was averaged on-board into $5 \times 5$ blocks to create a 2.77 km (smooth) resolution and then reprojected onto a 30 arc-second grid.[3] Second, the data providers at NOAA processed the daily images into a single annual composite. As a result, many pixels suffering from top-coding in at least one of the underlying fine resolution data points or smooth resolution daily images would have ended up with an average value of less than 63. Hsu et al. (2015) suggest that this subtle type of top-coding may even start at a DN as low as 35. Since "the OLS does onboard averaging to produce its global coverage data, saturation does not happen immediately when radiance reaches the maximum level. On the contrary, as the actual radiance grows, the observed DN value fails to follow the radiance growth linearly, causing a gradual transition into a plateau of full saturation" (Hsu et al., 2015, p. 1872).

We explore the location of the top-coding threshold with a statistical approach. If only the stable lights at 63 DN were subject to top-coding, we would expect the histogram in panel (a) of Figure B-1 to show a decreasing shape ending in a spike only at 63 DN. Instead, we observe an increase in the number of pixels from 55 onwards (e.g. a bathtub shape), signaling that these values are top-coded as well. Further evidence along these lines is provided by panel (b) of Figure B-1. It shows a histogram of the light intensity of the stable lights DNs associated with high radiance-calibrated values (above 160 DN). There are a large number of pixels with DNs down to the mid-50s which correspond to very high radiance-calibrated values, but the density falls rapidly below the mid-50s. Other years show very similar patterns.

Table B-1 list the percentile values of the radiance-calibrated lights corresponding to stable lights at 55 DN, 56 DN, and so on. The stable lights at 63 DN have the highest radiance-calibrated values (50% of them are higher than 390 DN). But there is also a significant share of 55 DN lights corresponding to high radiance-calibrated values, for instance, 25% are recorded with 140 DN or brighter.

[3] See `https://directory.eoportal.org/web/eoportal/satellite-missions/d/dmsp-block-5d` or Abrahams et al. (2018) for a detailed description of the sensors and on-board processing.

**Figure B-1** – Histograms of stable lights in 1999

**(a)** If stable DN > 9 **(b)** If radiance-calibrated DN > 160

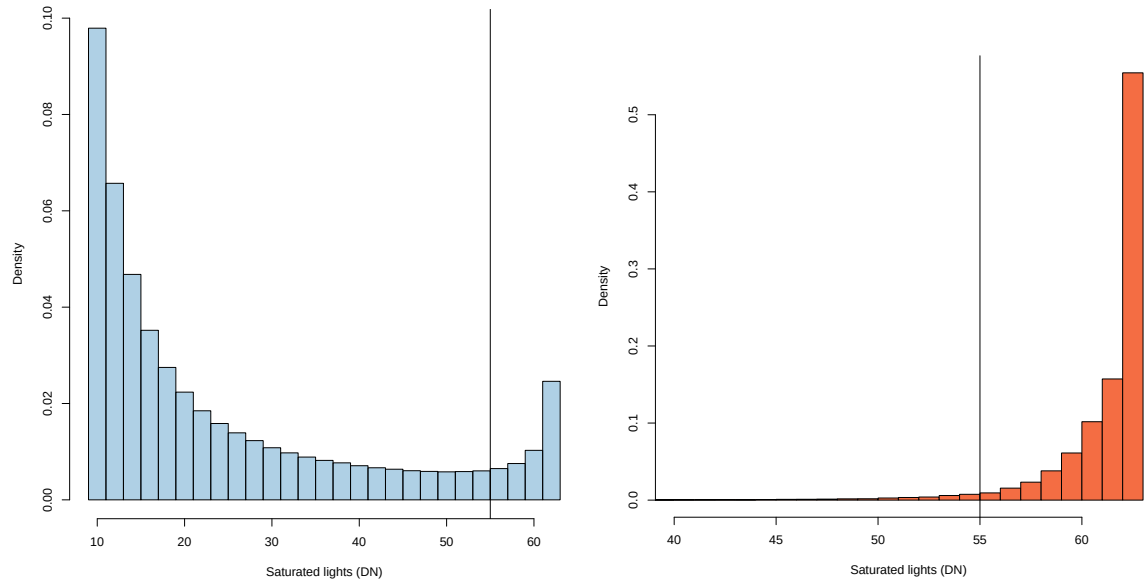


*Notes*: Illustration of the location of the top-coding threshold in the stable lights. Panel a) shows a histogram of the F12 satellite in 1999 for all pixels with a DN greater 9. Panel b) shows a histogram of the same satellite only for pixels where the radiance-calibrated light intensity is greater 160 DN. The input data are a 10% representative sample of all non-zero lights in the stable lights and radiance-calibrated data at the pixel level (see Elvidge et al., 2009, Hsu et al., 2015).

**Table B-1** – Percentiles of radiance-calibrated values at given stable lights values in 2000

| Stable lights | Radiance-calibrated percentiles | | | | | |
|---|---|---|---|---|---|---|
| DN | 5% | 25% | 50% | 75% | 95% | 99% |
| 55 | 53.20 | 74.94 | 99.41 | 140.85 | 232.90 | 328.86 |
| 56 | 56.15 | 79.99 | 108.20 | 153.92 | 250.93 | 344.05 |
| 57 | 60.14 | 84.99 | 115.11 | 164.63 | 262.18 | 357.60 |
| 58 | 64.13 | 92.81 | 125.35 | 179.57 | 277.59 | 392.33 |
| 59 | 70.32 | 101.97 | 141.92 | 203.17 | 306.77 | 423.28 |
| 60 | 79.16 | 116.64 | 163.92 | 231.91 | 344.57 | 497.25 |
| 61 | 89.33 | 137.89 | 196.68 | 268.21 | 410.91 | 625.30 |
| 62 | 109.03 | 176.36 | 246.66 | 331.46 | 524.18 | 762.63 |
| 63 | 160.91 | 276.92 | 390.08 | 560.28 | 952.14 | 1494.85 |

*Notes*: The table reports values from the cumulative distribution function of the radiance-calibrated lights which are associated with a given stable lights value (from 55 to 63). For instance, 25% of the radiance-calibrated values associated with a stable lights value of 61 DN, are below 137.89. The data are a representative 10% sample for the year 2000.

# C Additional results for the model

## C.1 Proofs

In this section, we provide additional proofs of the model presented in the main text.

**The CDF of the number of rings:** Note that $r = \pi^{-1/2} x^{1/(2\phi)}$ implies $x = \pi^{\phi} r^{2\phi}$ and $\mathrm{d}x = 2\phi\pi^{\phi} r^{2\phi-1}\mathrm{d}r$. Substituting these definitions into eq. (1) and integrating yields the CDF of the number of rings per city as presented in eq. (2) of the main text

$$\begin{aligned} F(r) &= 2\phi x_c \pi^{-\phi} \int_{\tilde{r}}^{r} r^{-2\phi-1}\mathrm{d}r = 2\phi x_c \pi^{-\phi} \left[-\frac{1}{2\phi} r^{-2\phi}\right]_{\tilde{r}}^{r} \\ &= \begin{cases} 0 \text{ for } r < \tilde{r} = \pi^{-1/2} x_c^{1/(2\phi)} \\ 1 - y_c \pi^{-\phi} r^{-2\phi} \text{ for } r >= \tilde{r} = \pi^{-1/2} x_c^{1/(2\phi)}. \end{cases} \end{aligned} \tag{C-1}$$

**The density of pixels:** Start with the distribution of the number of pixels. At distances $d < \tilde{d}$, the amount of pixels increases linearly in $d$ as rings farther away from the center contain more pixels: $\frac{\mathrm{d}}{\mathrm{d}d}\pi d^2 = 2\pi d$. Beyond $\tilde{d}$, the effect within each city has to be multiplied by the survival function $1 - F(r)$ from eq. (2), as there are fewer and fewer cities of such size. Denoting the number of cities as $M$, the absolute amount of pixels $N$ as a function of $d$ is

$$P(d) = \begin{cases} 2\pi d M \text{ for } d < \tilde{d} = \pi^{-1/2} x_c^{1/(2\phi)} \\ 2\pi^{1-\phi} M x_c d^{1-2\phi} \text{ for } d \geq \tilde{d} = \pi^{-1/2} x_c^{1/(2\phi)}. \end{cases} \tag{C-2}$$

The total number of pixels, $N$, can be obtained by integration

$$\begin{aligned} N &= \int_0^{\tilde{d}} 2\pi d M \mathrm{d}d + \int_{\tilde{d}}^{\infty} 2\pi^{1-\phi} M x_c d^{1-2\phi} \mathrm{d}d = 2\pi M \left[\frac{1}{2} d^2\right]_0^{\tilde{d}} + 2\pi^{1-\phi} M x_c \left[\frac{1}{2-2\phi} d^{2-2\phi}\right]_{\tilde{d}}^{\infty} \\ &= \pi M \frac{y_c^{1/\phi}}{\pi} + \frac{\pi^{1-\phi} M y_c}{\phi - 1} \left(\frac{y_c^{1/\phi}}{\pi}\right)^{1-\phi} = M x_c^{1/\phi} + \frac{1}{\phi - 1} M x_c^{1/\phi} = \frac{\phi}{\phi - 1} M x_c^{1/\phi}. \end{aligned} \tag{C-3}$$

Dividing eq. (C-2) by $N$ yields the density, $f(d)$, shown in eq. (4):

$$f(d) = \begin{cases} 2\pi \frac{\phi-1}{\phi} x_c^{-1/\phi} d \text{ for } d < \tilde{d} \\ 2\pi^{1-\phi} \frac{\phi-1}{\phi} x_c^{1-1/\phi} d^{1-2\phi} \text{ for } d \geq \tilde{d} \end{cases} \tag{C-4}$$

with $\tilde{d} = \pi^{-1/2} x_c^{1/(2\phi)}$.

The density is illustrated in panel (a) of Figure 4 in the main text.

## C.2 The maxima distribution of city lights

When assuming that lights within cities follow the negative exponential distribution (assumption 4b), our expression for the overall top light distribution depends on the distribution of light maxima across cities. We discuss three cases for the distribution of light maxima, which is informed by empirical evidence on the distribution of the maxima of 988 world cities (above 500,000 inhabitants), measured by the radiance-calibrated lights in 2010. We will here provide further empirical tests to underpin case 3 that this distribution is Pareto in the tail.

Starting with the histogram in Figure 5, we see a downward-sloping shape from around luminosity values of 500. We will therefore test for a Pareto tail using five different thresholds (500, 600, 700, 800, 900).

We follow Cirillo (2013) in drawing a discriminant moment ratio plot to provide evidence of the Pareto property. Figure C-1 plots the coordinate pair of the coefficient of variation (i.e., standard deviation divided by the mean) on the $x$-axis and skewness on the $y$-axis. As each parametric distribution has its particular curve of feasible coordinates, the plane can be divided into a Pareto area (comprising Pareto type I and II), a log-normal area and a gray area possibly belonging to both. Here we see that no matter which threshold we choose, the distribution of maximum light intensities across cities falls in the Pareto area.

Next, we estimate the Pareto coefficient of the maxima distribution. We run log-rank regressions with both the OLS and Hill estimator for the different thresholds, following the literature (see for instance Gabaix and Ibragimov, 2011). As Table C-1 shows, the Pareto coefficient is rather high, ranging from 2.6 to 3.5 depending on the threshold and estimator. While being Pareto, light maxima across cities are therefore rather equally distributed, compared to, for example, the overall light distribution. Also, we note that there is a slight increase in the Pareto $\alpha$ as the threshold increases and there are fewer observations left. But overall, the magnitude of the coefficients is rather stable.

**Figure C-1** – Discriminant moment ratio plot for distribution of maxima

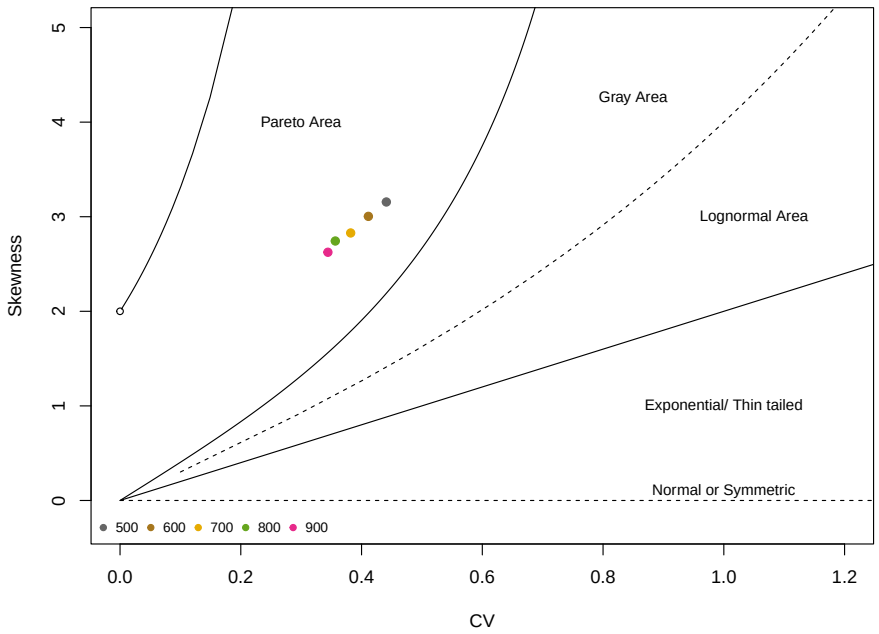


*Notes*: The panels show discriminant moment ratio plots (Cirillo, 2013) using various thresholds. The data are the distribution of maximum light intensities in 988 world cities above 500,000 inhabitants, measured by the radiance-calibrated satellite in 2010.

**Table C-1** – Rank regressions for the maxima distribution

| Threshold | 500 | 600 | 700 | 800 | 900 |
|---|---|---|---|---|---|
| *Panel a) OLS Estimator* | | | | | |
| Pareto $\hat{\alpha}$ | 2.7813 | 3.0096 | 3.1003 | 3.1985 | 3.4712 |
| (S.E.) | (0.0165) | (0.0183) | (0.0273) | (0.0347) | (0.0294) |
| Observations | 278 | 187 | 120 | 83 | 64 |
| *Panel b) Hill Estimator* | | | | | |
| Pareto $\hat{\alpha}$ | 2.6305 | 2.8977 | 2.9465 | 2.9717 | 3.3506 |
| (S.E.) | (0.1572) | (0.2129) | (0.2679) | (0.3282) | (0.4222) |
| Observations | 281 | 188 | 122 | 83 | 64 |

*Notes*: The table reports the results of rank regressions with $\log(\text{rank}(y_i) - 1/2) - \log N$ as the dependent variable. Asymptotic standard errors computed as $(2/N)^{1/2}\hat{\alpha}$ are reported in parentheses (see Gabaix and Ibragimov, 2011).

# D Extreme value theory

As an alternative to our stylized urban economics model, we can also motivate a Pareto distribution in top lights purely on statistical grounds using extreme value theory (EVT). EVT deals with the probability distributions of sparse observations such as threshold exceedances. A key result of this theory is that these quantities observe a Generalized Pareto distribution (Coles, 2001).

More precisely, let $X_1, X_2, \ldots$ be a sequence of independent random variables—such as light—with common but unknown distribution function $F$, and let $M_n = \max\{X_1, \ldots, X_n\}$. If $F$ satisfies the *extremal types theorem* (Coles, 2001), so that for large $n$, $\mathbb{P}[M_n > z] \approx G(z)$ with $G(z)$ as the Generalized Extreme Value distribution, then, for a high enough threshold $u$, the distribution of the threshold exceedance $\mathbb{P}[(X - u) > y | X > u]$ is approximately

$$H(y) = 1 - \left(1 + \frac{\xi y}{\tilde{\sigma}}\right)^{-\frac{1}{\xi}}, \tag{D-1}$$

no matter which regular distribution $X$ was drawn from.

This means that we will observe a Generalized Pareto distribution with parameters $\xi$ and $\sigma$ for all lights values above a specified threshold. With $\xi = 0$, this reduces to the exponential distribution and with $\xi > 0$ the distribution is Pareto. There is strong evidence that the latter case holds for the lights data.

Figure D-1 plots the Generalized Pareto distribution against the empirical distribution function of the radiance-calibrated data from 2010. It visualizes the close fit.

Table D-1 shows the results of fitting the Generalized Pareto distribution to various top shares of the light distribution of the seven satellite-years of radiance-calibrated data. The fit is very good and the estimated $\xi$ parameters are always significantly positive. This clearly points towards a Pareto distribution.

**Figure D-1** – Generalized Pareto CDF versus EDF, radiance-calibrated data in 2010

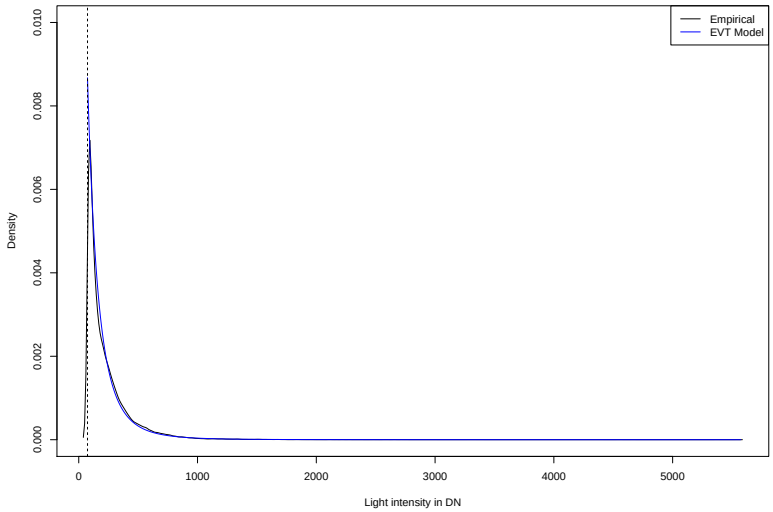


*Notes*: Illustration of Generalized Pareto CDF fitted to the data and the empirical distribution function (EDF). The EDF and Generalized Pareto CDF are fitted to the top 4% of stable lights in 2010. The input data are a 10% representative sample of all non-zero lights of the radiance-calibrated data at the pixel level, where each pixel is $30 \times 30$ arc seconds.

**Table D-1** – Fitted Generalized Pareto distributions, varying thresholds

| Year | 1996 | 1999 | 2000 | 2003 | 2004 | 2006 | 2010 | Average |
|---|---|---|---|---|---|---|---|---|
| | | | | *Panel a) Top 5%* | | | | |
| $\ln \sigma$ | 4.8260 | 4.8674 | 5.0702 | 4.9841 | 4.9127 | 4.7153 | 4.6387 | 4.8592 |
| | (0.0069) | (0.0060) | (0.0060) | (0.0063) | (0.0061) | (0.0062) | (0.0058) | [0.14915] |
| $\xi$ | 0.2266 | 0.1753 | 0.1387 | 0.1629 | 0.1356 | 0.0944 | 0.1601 | 0.1562 |
| | (0.0056) | (0.0047) | (0.0045) | (0.0049) | (0.0047) | (0.0047) | (0.0042) | [0.0407] |
| Threshold | 98 | 114 | 131 | 154 | 150 | 123 | 1208 | – |
| Observations | 58,010 | 70,112 | 64,110 | 60,057 | 64,133 | 59,691 | 64,646 | – |
| | | | | *Panel b) Top 4%* | | | | |
| $\ln \sigma$ | 4.9510 | 4.9405 | 5.1105 | 5.0402 | 4.9532 | 4.7495 | 4.6639 | 4.9155 |
| | (0.0073) | (0.0064) | (0.0065) | (0.0068) | (0.0066) | (0.0068) | (0.0063) | [0.1569] |
| $\xi$ | 0.1736 | 0.1508 | 0.1302 | 0.1476 | 0.1837 | 0.1301 | 0.0902 | 0.1438 |
| | (0.0057) | (0.0049) | (0.0048) | (0.0052) | (0.0051) | (0.0051) | (0.0046) | [0.0310] |
| Threshold | 118 | 136 | 160 | 180 | 175 | 143 | 127 | – |
| Observations | 48,342 | 58,426 | 53,407 | 50,047 | 53,443 | 49,743 | 53,872 | – |
| | | | | *Panel c) Top 3%* | | | | |
| $\ln \sigma$ | 5.0520 | 5.0042 | 5.1151 | 5.0807 | 4.9771 | 4.7847 | 4.6836 | 4.9568 |
| | (0.0079) | (0.0070) | (0.0073) | (0.0076) | (0.0075) | (0.0075) | (0.0070) | [0.1614] |
| $\xi$ | 0.1355 | 0.1332 | 0.1438 | 0.1432 | 0.1933 | 0.1266 | 0.0903 | 0.1380 |
| | (0.0060) | (0.0053) | (0.0055) | (0.0057) | (0.0058) | (0.0056) | (0.0050) | [0.0304] |
| Threshold | 147 | 166 | 199 | 215 | 208 | 169 | 151 | – |
| Observations | 38,673 | 46,742 | 42,740 | 40,039 | 42,755 | 39,795 | 43,097 | – |
| | | | | *Panel d) Top 2%* | | | | |
| $\ln \sigma$ | 5.1175 | 5.0606 | 5.1446 | 5.1170 | 5.0064 | 4.8095 | 4.6943 | 4.9928 |
| | (0.0090) | (0.0080) | (0.0086) | (0.0088) | (0.0088) | (0.0088) | (0.0081) | [0.1739] |
| $\xi$ | 0.1198 | 0.1222 | 0.1508 | 0.1459 | 0.2091 | 0.1330 | 0.0981 | 0.1398 |
| | (0.0069) | (0.0060) | (0.0065) | (0.0066) | (0.0069) | (0.0066) | (0.0059) | [0.0353] |
| Threshold | 191 | 209 | 248 | 262 | 252 | 204 | 183 | – |
| Observations | 29,006 | 35,057 | 32,055 | 30,029 | 32,067 | 29,845 | 32,324 | – |
| | | | | *Panel e) Top 1%* | | | | |
| $\ln \sigma$ | 5.2035 | 5.1025 | 5.2287 | 5.1729 | 5.1013 | 4.8650 | 4.7009 | 5.0535 |
| | (0.0109) | (0.0099) | (0.0103) | (0.0108) | (0.0109) | (0.0108) | (0.0100) | [0.1966] |
| $\xi$ | 0.0961 | 0.1262 | 0.1374 | 0.1483 | 0.2037 | 0.1324 | 0.1163 | 0.1370 |
| | (0.0082) | (0.0074) | (0.0078) | (0.0082) | (0.0086) | (0.0082) | (0.0074) | [0.0337] |
| Threshold | 259 | 275 | 319 | 332 | 315 | 255 | 230 | – |
| Observations | 19,337 | 23,371 | 21,370 | 20,019 | 21,378 | 19,897 | 21,548 | – |

*Notes:* The table reports parameter estimates from fitting the Generalized Pareto distribution shown in eq. (D-1). The input data are a 10% representative sample of all non-zero lights in the radiance-calibrated data above the defined threshold at the pixel level, where each pixel is $30 \times 30$ arc seconds. The last column reports the point average of the seven satellites and its standard deviation in brackets.

# E Additional results using the radiance-calibrated data

This section complements the analysis in the paper by providing additional robustness checks of our Pareto hypothesis using the seven satellite-years of radiance-calibrated data.

**Visual Inspection:** Panel (a) of Figure E-1 shows Zipf plots for the top 2% of lights for each of the seven satellite-years of radiance-calibrated data. A Zipf plot is a visualization of the Pareto survival function in logs. A linear Zipf plot is usually considered evidence in favor of the Pareto distribution, but its practical relevance is being contested (Cirillo, 2013). Our plots for the lights data are qualitatively similar to those of the top incomes literature, in that they display linear sections together with some initial curvature and outliers at the end.[4] It is well-known that Zipf plots often deviate from linearity at the very top since fewer and fewer values are observed at the extremes. Sometimes this is addressed by removing the very top. We use logarithmic bins so that the size of the bins increases by a multiplicative factor (Newman, 2005). The sensitivity of Zipf plots to outliers is compounded by instability and measurement errors afflicting the radiance-calibrated satellites. While we conclude that the Zipf plot using the radiance-calibrated data is ambiguous, we obtain a near-linear Zipf plot using the superior VIIRS data (see the next section).

Panel (b) of Figure E-1 provides another graphical test for the Pareto distribution based on 'Van der Wijk's Law'. The Pareto distribution is unique in that the average above some level $y$ is proportional to $y$ at all points in the tail, with a factor of proportionality equal to $\frac{\alpha}{\alpha-1} > 1$. The graph plots, for each DN on the $x$-axis, the average luminosity of all pixels brighter than this value on the $y$-axis. As expected, we observe a linear relationship with a slope above unity.

**Tests against the log-normal distribution:** As a robustness check, we pit the Pareto distribution against other plausible candidates. We pay particular attention to the log-normal distribution, since it is commonly used to describe the complete distribution of incomes or city sizes. Table E-1 shows the results from separate regressions of the empirical distribution function on the Pareto CDF and the log-normal CDF based on the top 4% of the data. The estimated coefficient for the Pareto CDF is closer to unity and the $R^2$ is substantially larger than in the log-normal counterpart (0.98 vs. 0.83). Figure E-2 visualizes this difference in fit for the year 2010. The log-normal CDF fits the data poorly, while the Pareto CDF is always closer to the empirical distribution.

[4] Working with any top share, from the top 5% to the top 1% gives qualitatively similar results, even if the case for a Pareto distribution tends to be stronger the higher we set the threshold. This is in line with the empirical literature on Pareto applications in other fields.

**Unrestricted rank regressions:** Recall that for Pareto-distributed observations $y_i$, $i = 1, ...N$, we have $\text{rank}(y_i) \approx N y_c^{\alpha} y_i^{-\alpha}$, or, in logarithms $\log \text{rank}(y_i) - \log N \approx \alpha \log y_c - \alpha \log y_i$. Hence, in the regression

$$\log\Big(\text{rank}(y_i) - \frac{1}{2}\Big) - \log N = \alpha_1 \log y_c + \alpha_2 \log y_i + \epsilon \tag{E-1}$$

only the Pareto distribution satisfies the null hypothesis that $-\alpha_1 = \alpha_2$ with $\alpha_2 < 0$. As before, we follow Gabaix and Ibragimov (2011) and subtract one half from the rank to improve the OLS estimation of the tail exponent in the rank regression.

Table E-2 reports the OLS rank regression results of eq. (E-1) for all seven satellites at various different thresholds, i.e. the top 5% to top 1%. The two coefficients are usually very close and the $R^2$s are high (0.96–0.99).[5]

**The Hill estimator:** If the null hypothesis $-\alpha_1 = \alpha_2 = \alpha$ is enforced in eq. (E-1), one can directly obtain the parameter estimate for the Pareto $\alpha$. In the main text we estimate this parameter using OLS rank regressions. As a robustness check, we now use the Hill estimator (Hill, 1975), $\hat{\alpha}_{Hill} = (N-1)\left(\sum_{i=1}^{N-1} \log y_i - \log y_c\right)^{-1}$, for the restricted rank regression

$$\log \text{rank}(y_i) - \log N \approx \alpha \log y_c - \alpha \log y_i. \tag{E-2}$$

Under the assumption of a Pareto distribution, the Hill estimator equals the efficient maximum likelihood estimator and is known for its superior properties for fitting the tail of the Pareto distribution (Eeckhout, 2009). The standard errors are given by $\hat{\alpha}_{Hill}/\sqrt{N-3}$ (see Gabaix, 2009).

Table E-3 report the results for all seven satellites at various different thresholds, i.e. the top 5% to top 1%. The Pareto parameters obtained using the Hill estimator are very similar to the OLS estimates in the main text. For the top 3-4%, the values are between 1.3 and 1.6 for the seven satellites, very close to the average OLS parameter estimate of 1.5. For higher thresholds, we observe also the same increase in the parameter estimate that we observe in the OLS results.

[5]Note that formal statistical tests, e.g. tests of coefficient equality or Kolmogorov-Smirnoff tests, do not make much sense in huge samples such as ours. Gabaix and Ioannides (2004, p. 2350) capture this nicely: "with an infinitely large dataset one can reject any non-tautological theory." The extremely small standard errors lead to overrejections of the null hypothesis unless the empirical value equals exactly the theoretical value.

**Figure E-1** – Zipf plot and Van der Wijk's plot

**(a)** Zipf **(b)** Van der Wijk

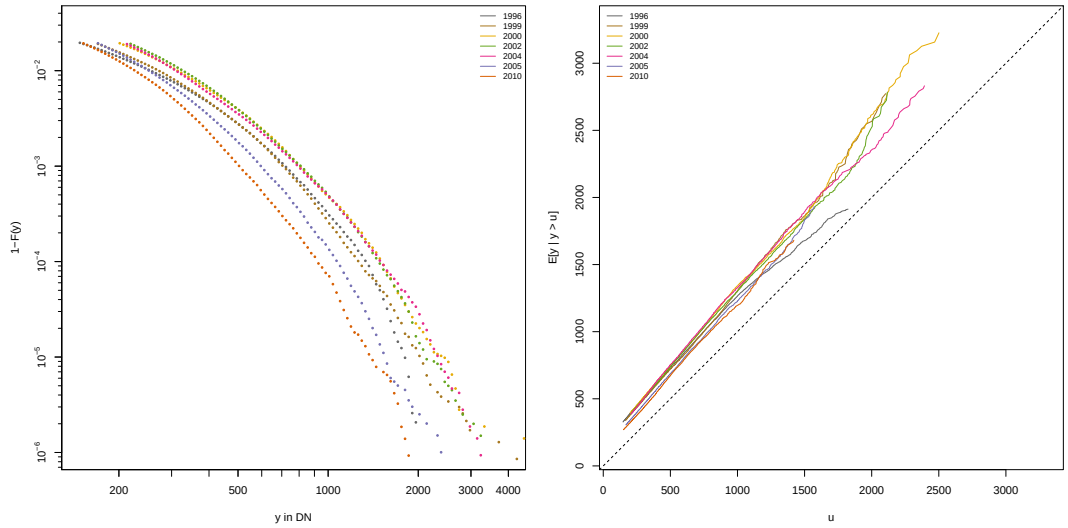


*Notes*: Popular graphical tests for an approximate Pareto distribution in top lights. Panel (a) shows the Zipf plot for the top 2% of all pixels. The figure uses logarithmic binning to reduce noise and sampling errors in the right tail of the distribution (see Newman, 2005). There are about 100 bins in the tail, where the exact number depends on the range of the input data. Panel (b) demonstrates Van der Wijk's law, which states that the average light above some value $u$ is proportional to $u$, this is $\mathrm{E}[y|y > u] \propto u$. Here, too, the data is the top 2% of all pixels. The input data are a 10% representative sample of all non-zero lights in the radiance-calibrated data at the pixel level.

**Figure E-2** – Pareto and log-normal CDF versus EDF, radiance-calibrated lights in 2010

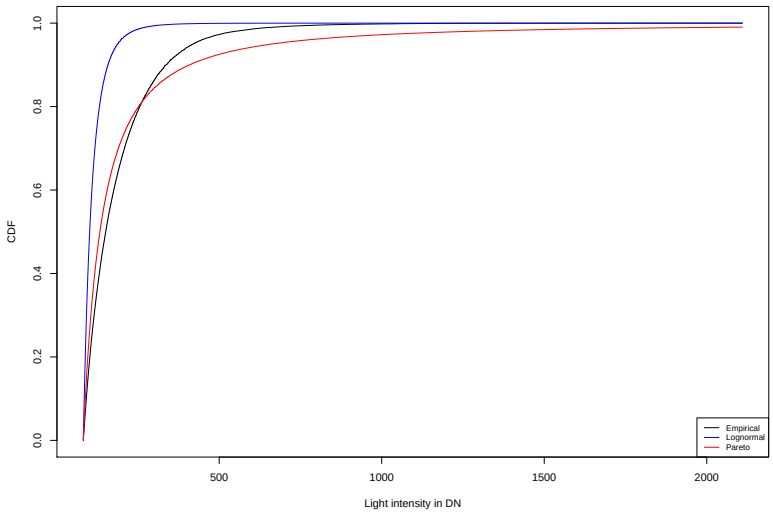


*Notes*: Illustration of the difference between the Pareto and log-normal CDFs fitted to the data and the empirical distribution function (EDF). Note that the log-normal distribution was fitted to the whole distribution rather than the tail because of its unimodal shape, while the Pareto distribution is estimated only on the tail. For comparison, we adjust the CDFs so that they all start at the top 4% of radiance-calibrated lights in 2010. The input data are a 10% representative sample of all non-zero lights in the radiance-calibrated data at the pixel level, where each pixel is $30 \times 30$ arc seconds.

**Table E-1** – Regression of the EDF on theoretical CDFs, top 4%

| Year | 1996 | 1999 | 2000 | 2003 | 2004 | 2006 | 2010 | Average |
|---|---|---|---|---|---|---|---|---|
| | *Panel a) Pareto CDF on RHS* | | | | | | | |
| Slope | 1.0108 | 1.0551 | 1.0616 | 1.0575 | 1.0746 | 1.0722 | 1.0796 | 1.0588 |
| | (0.0003) | (0.0004) | (0.0005) | (0.0004) | (0.0004) | (0.0005) | (0.0005) | [0.0231] |
| Constant | -0.0320 | -0.0668 | -0.0746 | -0.0666 | -0.0787 | -0.0784 | -0.0858 | -0.0690 |
| | (0.0002) | (0.0002) | (0.0003) | (0.0002) | (0.0003) | (0.0003) | (0.0003) | [0.0177] |
| $R^2$ | 0.9914 | 0.9866 | 0.9802 | 0.9884 | 0.9869 | 0.9860 | 0.9831 | – |
| | *Panel b) Log-normal CDF on RHS* | | | | | | | |
| Slope | 0.9004 | 0.9265 | 0.9181 | 0.9387 | 0.9520 | 0.9472 | 0.9488 | 0.9331 |
| | (0.0014) | (0.0016) | (0.0018) | (0.0014) | (0.0014) | (0.0014) | (0.0015) | [0.0190] |
| Constant | -0.1653 | -0.2186 | -0.2238 | -0.1954 | -0.2088 | -0.2031 | -0.2179 | -0.2047 |
| | (0.0011) | (0.0013) | (0.0015) | (0.0011) | (0.0011) | (0.0011) | (0.0012) | [0.0200] |
| $R^2$ | 0.8496 | 0.7913 | 0.7626 | 0.8508 | 0.8467 | 0.8480 | 0.8268 | – |

*Notes*: The table reports results of a regression of the empirical distribution function (EDF) on the Pareto or log-normal CDF, using the top 4% of the data. The data are a 10% representative sample of all non-zero lights in the radiance-calibrated data at the pixel level, where each pixel is $30 \times 30$ arc seconds. The last column reports the point average of the seven satellites and its standard deviation in brackets.

**Table E-2** – Unrestricted rank regressions

| Year | 1996 | 1999 | 2000 | 2003 | 2004 | 2006 | 2010 | Average |
|---|---|---|---|---|---|---|---|---|
| | | | | *Panel a) Top 5%* | | | | |
| $y_i$ | -1.4334 | -1.4996 | -1.4630 | -1.6903 | -1.6933 | -1.7388 | -1.7170 | -1.6050 |
| | (0.0012) | (0.0012) | (0.0013) | (0.0013) | (0.0013) | (0.0014) | (0.0015) | [0.1330] |
| $y_c$ | 1.4736 | 1.5632 | 1.5318 | 1.7539 | 1.7582 | 1.8087 | 1.7936 | 1.6690 |
| | (0.0014) | (0.0015) | (0.0016) | (0.0016) | (0.0015) | (0.0017) | (0.0018) | [0.1405] |
| $R^2$ | 0.9694 | 0.9651 | 0.9600 | 0.9701 | 0.9721 | 0.9677 | 0.9620 | 0.9666 |
| Observations | 96,685 | 116,858 | 106,914 | 100,095 | 106,899 | 99,487 | 107,745 | 104,955 |
| | | | | *Panel b) Top 4%* | | | | |
| $y_i$ | -1.5130 | -1.6328 | -1.6165 | -1.8403 | -1.8513 | -1.9101 | -1.9056 | -1.7528 |
| | (0.0015) | (0.0014) | (0.0016) | (0.0016) | (0.0014) | (0.0017) | (0.0018) | [0.1612] |
| $y_c$ | 1.5618 | 1.6974 | 1.6870 | 1.8978 | 1.9132 | 1.9767 | 1.9804 | 1.8163 |
| | (0.0017) | (0.0017) | (0.0019) | (0.0018) | (0.0016) | (0.0019) | (0.0020) | [0.1655] |
| $R^2$ | 0.9662 | 0.9661 | 0.9623 | 0.9725 | 0.9759 | 0.9711 | 0.9658 | 0.9685 |
| Observations | 77,348 | 93,484 | 85,482 | 80,075 | 85,489 | 79,590 | 86,196 | 83,952 |
| | | | | *Panel c) Top 3%* | | | | |
| $y_i$ | -1.6609 | -1.8385 | -1.8624 | -2.0491 | -2.0633 | -2.1470 | -2.1746 | -1.9708 |
| | (0.0019) | (0.0018) | (0.0019) | (0.0019) | (0.0016) | (0.0020) | (0.0021) | [0.1882] |
| $y_c$ | 1.7225 | 1.9017 | 1.9340 | 2.1044 | 2.1174 | 2.2068 | 2.2429 | 2.0328 |
| | (0.0022) | (0.0020) | (0.0022) | (0.0021) | (0.0018) | (0.0022) | (0.0024) | [0.1872] |
| $R^2$ | 0.9646 | 0.9695 | 0.9691 | 0.9761 | 0.9811 | 0.9762 | 0.9721 | 0.9727 |
| Observations | 58,011 | 70,115 | 64,111 | 60,058 | 64,134 | 59,692 | 64,647 | 62,967 |
| | | | | *Panel d) Top 2%* | | | | |
| $y_i$ | -1.9711 | -2.1628 | -2.2315 | -2.3687 | -2.3478 | -2.4809 | -2.5663 | -2.3042 |
| | (0.0025) | (0.0023) | (0.0022) | (0.0023) | (0.0018) | (0.0024) | (0.0025) | [0.2009] |
| $y_c$ | 2.0329 | 2.2180 | 2.2831 | 2.4156 | 2.3880 | 2.5295 | 2.6215 | 2.3555 |
| | (0.0029) | (0.0025) | (0.0025) | (0.0025) | (0.0020) | (0.0026) | (0.0027) | [0.1974] |
| $R^2$ | 0.9698 | 0.9757 | 0.9798 | 0.9825 | 0.9871 | 0.9826 | 0.9807 | 0.9797 |
| Observations | 38,673 | 46,742 | 42,740 | 40,039 | 42,756 | 39,794 | 43,097 | 41,977 |
| | | | | *Panel e) Top 1%* | | | | |
| $y_i$ | -2.5471 | -2.7216 | -2.7241 | -2.8508 | -2.7006 | -2.9769 | -3.1652 | -2.8123 |
| | (0.0039) | (0.0031) | (0.0031) | (0.0030) | (0.0027) | (0.0032) | (0.0029) | [0.2049] |
| $y_c$ | 2.5922 | 2.7593 | 2.7596 | 2.8823 | 2.7258 | 3.0097 | 3.2005 | 2.8471 |
| | (0.0043) | (0.0034) | (0.0034) | (0.0033) | (0.0029) | (0.0035) | (0.0031) | [0.2031] |
| $R^2$ | 0.9781 | 0.9849 | 0.9864 | 0.9889 | 0.9895 | 0.9886 | 0.9911 | 0.9868 |
| Observations | 19,337 | 23,373 | 21,372 | 20,020 | 21,377 | 19,898 | 21,551 | 20,990 |

*Notes*: The table reports OLS results obtained from the unrestricted rank regressions eq. (E-1) at various relative thresholds. The input data are a 10% representative sample of all non-zero lights in the radiance-calibrated data above the defined threshold at the pixel level, where each pixel is $30 \times 30$ arc seconds. Standard errors are in parentheses. The last column reports the point average of the seven satellites and its standard deviation in brackets.

**Table E-3** – Parameter estimates from rank regressions (Hill estimator)

| Year | 1996 | 1999 | 2000 | 2003 | 2004 | 2006 | 2010 | Average |
|---|---|---|---|---|---|---|---|---|
| | | | | *Panel a) Top 5%* | | | | |
| Pareto $\hat{\alpha}$ | 1.2286 | 1.1833 | 1.1289 | 1.3112 | 1.3100 | 1.3356 | 1.3012 | 1.2570 |
| | (0.0040) | (0.0035) | (0.0035) | (0.0041) | (0.0040) | (0.0042) | (0.0040) | [0.0780] |
| Observations | 96,685 | 116,858 | 106,914 | 100,095 | 106,899 | 99,487 | 107,745 | – |
| | | | | *Panel b) Top 4%* | | | | |
| Pareto $\hat{\alpha}$ | 1.2487 | 1.2689 | 1.2233 | 1.4431 | 1.4315 | 1.4666 | 1.4333 | 1.3593 |
| | (0.0045) | (0.0042) | (0.0042) | (0.0051) | (0.0049) | (0.0052) | (0.0049) | [0.1065] |
| Observations | 77,348 | 93,484 | 85,482 | 80,075 | 85,489 | 79,590 | 86,196 | – |
| | | | | *Panel c) Top 3%* | | | | |
| Pareto $\hat{\alpha}$ | 1.2948 | 1.4152 | 1.3805 | 1.6023 | 1.6234 | 1.6672 | 1.6478 | 1.5188 |
| | (0.0054) | (0.0053) | (0.0055) | (0.0065) | (0.0064) | (0.0068) | (0.0065) | [0.1509] |
| Observations | 58,011 | 70,115 | 64,111 | 60,058 | 64,134 | 59,692 | 64,647 | – |
| | | | | *Panel d) Top 2%* | | | | |
| Pareto $\hat{\alpha}$ | 1.5068 | 1.6869 | 1.7536 | 1.8920 | 1.9325 | 1.9860 | 2.0095 | 1.8239 |
| | (0.0077) | (0.0078) | (0.0085) | (0.0095) | (0.0093) | (0.0100) | (0.0097) | [0.1832] |
| Observations | 38,673 | 46,742 | 42,740 | 40,039 | 42,756 | 39,794 | 43,097 | – |
| | | | | *Panel e) Top 1%* | | | | |
| Pareto $\hat{\alpha}$ | 2.0363 | 2.2458 | 2.2613 | 2.4101 | 2.3582 | 2.5190 | 2.6558 | 2.3552 |
| | (0.0146) | (0.0147) | (0.0155) | (0.0170) | (0.0161) | (0.0179) | (0.0181) | [0.2011] |
| Observations | 19,337 | 23,373 | 21,372 | 20,020 | 21,377 | 19,898 | 21,551 | – |

*Notes*: The table reports the results of the restricted rank regression eq. (E-2) using the Hill estimator. The data are a 10% representative sample of all non-zero lights in the radiance-calibrated data at the pixel level, where each pixel is $30 \times 30$ arc seconds. The last column reports the point average of the seven satellites and its standard deviation in brackets.

# F Additional results using the VIIRS data

Since October 2011, the first satellite of the Suomi National Polar Partnership Visible Infrared Imagining Radiometer Suite (NPP-VIIRS) has been in orbit. The VIIRS day-night-band (DNB) on-board sensors have a much higher native resolution of 15 arc seconds, are radiometrically calibrated, do not suffer from top-coding, and record a physical quantity (radiance). This section complements the analysis in the paper by providing additional robustness checks of our Pareto hypothesis using this new data.

Although the new system is undoubtedly superior in many respects, comparability with the previous series is limited for at least two reasons: *i)* the first annual VIIRS composite made available by NOAA refers to the year 2015, so that there is no temporal overlap with the 1992-2013 DMSP-OLS series, *ii)* the VIIRS satellites have an overpass time around midnight, in contrast to the evening hours of the DMSP-OLS satellites, so that it is not entirely clear what kind of production and consumption activity they capture (Elvidge et al., 2014, Nordhaus and Chen, 2015). While we do not rely on the VIIRS data for our replacement procedure, we use the first VIIRS cross-section from 2015 as another robustness check for whether the Pareto distribution holds. The VIIRS data are particularly insightful in this respect because of their superior quality.

To compare the higher resolution VIIRS image to the DMSP data, we resample the raster to the DMSP resolution and then extract radiances of each pixel at the locations of the 10% sample that we have been using thus far. Naturally, there are considerable differences in the scale since the VIIRS-DNB records radiance. Note that radiance is measured in nano watt per steradian per square centimeter ($10^{-9} W cm^{-2} sr^{-1}$). The difference in scale is reflected in the summary statistics of the VIIRS data. The mean is 3.98, the standard deviation is 18.65, and the maximum is 6567.42. The spatial Gini is much higher using the VIIRS data than in the radiance-calibrated data (0.79 vs. 0.60-0.65) which is owed to their improved sensors and finer resolution. Nevertheless, the top tail of the light distribution essentially exhibits the same properties.

Figure F-1 shows the Zipf plot for the VIIRS data. The shape is nearly linear, even high up in the tail and displays less curvature than the corresponding plot for the radiance-calibrated data. This also suggests that the radiance calibration process introduces noise and understates the Paretian nature of night lights.

Figure F-2 replicates a variant of the first figure of the paper by comparing the (normalized) light intensities indicated by the corrected data in 1999 to those recorded by the VIIRS DNB instrument in 2015. We downsampled the VIIRS data to the same resolution as the DMSP data by averaging the higher resolution pixels. The figure shows that the city profiles for the two mature cities (New York and London) are similar, even though the instruments, underlying scales, overpass times, and reference years differ. For New Delhi and Johannesburg, there is some discrepancy in the relative brightness of

sub-centers which may be due to recent developments or fundamental differences in how the data is recorded. As expected, the corrected data is considerably smoother than the VIIRS data, as it is derived from the radiance-calibrated data, which has both a much wider ground footprint and is subject to blooming (overglow).

Table F-1 replicates the results of the rank regressions using the VIIRS data. The results are qualitatively similar to those obtained with the radiance-calibrated data, but some small differences are notable. In particular, the estimated shape parameters are a bit higher for top shares of 3% to 5% but then also appear to be more stable in the upper tail. Since the VIIRS data are from five years after the most recent radiance-calibrated image and have a different overpass time, it is difficult to identify the source of these discrepancies.

**Figure F-1** – Zipf plot using the top 2% of pixels in the VIIRS data

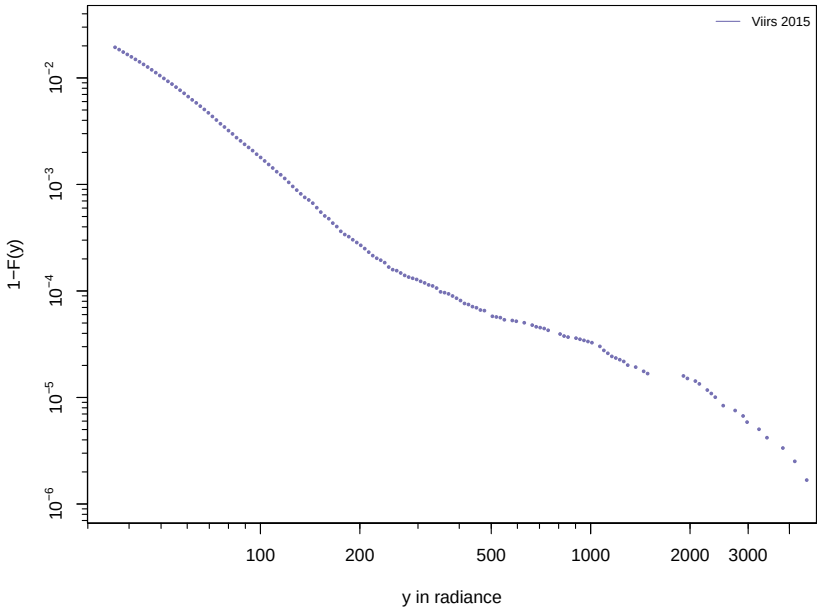


*Notes*: The figure shows a Zipf plot for the top 2% of all pixels of the VIIRS data, after resampling the data to the DMSP-OLS grid and resolution. The figure uses logarithmic binning to reduce noise and sampling errors in the right tail of the distribution (see Newman, 2005). There are about 140 bins in the tail, where the exact number depends on the range of the input data. The VIIRs pixels correspond to the same 10% representative sample of all non-zero lights in the radiance-calibrated data at the pixel level obtained from Hsu et al. (2015) and used in the rest of the paper.

**Figure F-2** – Corrected lights in 1999 versus VIIRS in 2015

**(a)** New York City

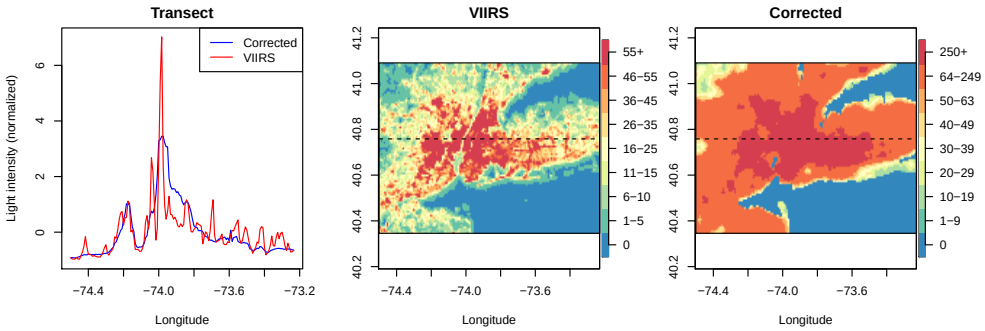


**(b)** London

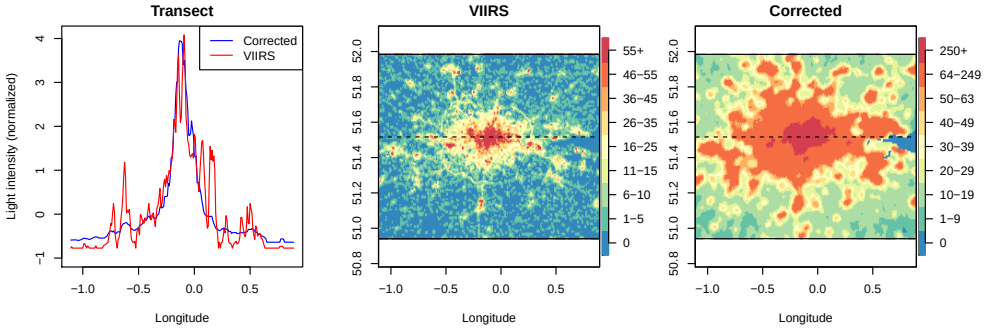


**(c)** New Delhi

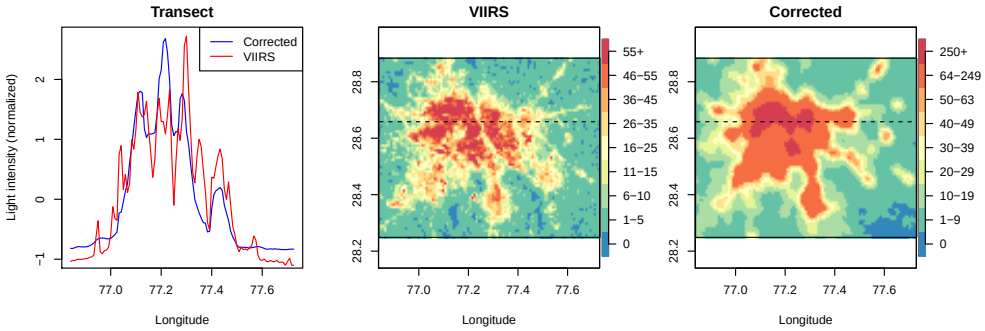


**(d)** Johannesburg

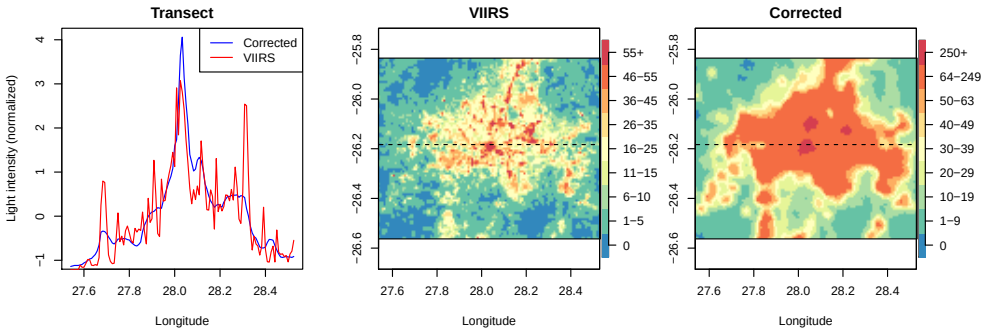


*Notes*: Comparison of the light intensities recorded our corrected lights in 1999 (as in Figure 1 in the paper) and by the VIIRS satellite in 2015 within four major cities. The left panel show the normalized light intensity along a longitudinal transect through the brightest pixel in each city. The middle panel shows a map based on the VIIRS data (in $10^{-9} W cm^{-2} sr^{-1}$). The right panel shows the same map using the corrected data (in DN). Both data have been binned and the color scales were adjusted so as to be visually comparable. Dashed lines indicate the transect path.

**Table F-1** – Rank regressions based on the VIIRS data in 2015

| Unrestricted regressions | | | Hill estimates | | Restricted regressions |
|---|---|---|---|---|---|
| | | *Panel a) Top 5%* | | | |
| $y_i$ | -1.9603 | $\alpha$ | 1.5876 | $\alpha$ | 1.7331 |
| | (0.0013) | | (0.0065) | | (0.0100) |
| $y_c$ | 2.0405 | | | | |
| | (0.0015) | | | | |
| $R^2$ | 0.9879 | | | | |
| Observations | 59,633 | | 59,633 | | 59,633 |
| | | *Panel b) Top 4%* | | | |
| $y_i$ | -2.0831 | $\alpha$ | 1.7331 | $\alpha$ | 1.8747 |
| | (0.0013) | | (0.0079) | | (0.0121) |
| $y_c$ | 2.1479 | | | | |
| | (0.0015) | | | | |
| $R^2$ | 0.9909 | | | | |
| Observations | 47,705 | | 47,705 | | 47,705 |
| | | *Panel c) Top 3%* | | | |
| $y_i$ | -2.2150 | $\alpha$ | 1.9144 | $\alpha$ | 2.0419 |
| | (0.0014) | | (0.0101) | | (0.0153) |
| $y_c$ | 2.2622 | | | | |
| | 0.0016 | | | | |
| $R^2$ | 0.9933 | | | | |
| Observations | 35,780 | | 35,780 | | 35,780 |
| | | *Panel b) Top 2%* | | | |
| $y_i$ | -2.3438 | $\alpha$ | 2.1671 | $\alpha$ | 2.2481 |
| | (0.0017) | | (0.0140) | | (0.0206) |
| $y_c$ | 2.3665 | | | | |
| | (0.0019) | | | | |
| $R^2$ | 0.9939 | | | | |
| Observations | 23,854 | | 23,854 | | 23,854 |
| | | *Panel e) Top 1%* | | | |
| $y_i$ | -2.3778 | $\alpha$ | 2.4716 | $\alpha$ | 2.4235 |
| | (0.0033) | | (0.0226) | | (0.0314) |
| $y_c$ | 2.3682 | | | | |
| | (0.0036) | | | | |
| $R^2$ | 0.9888 | | | | |
| Observations | 11,927 | | 11,927 | | 11927 |

*Notes*: The table uses the VIIRS data to repeat three regressions which were conducted with the radiance-calibrated data before: the unrestricted OLS rank regression eq. (E-1) and the restricted regression eq. (E-2) using both the OLS and the Hill estimator. Standard errors are reported in paretheses. For the OLS restricted rank regression, these are the asymptotic standard errors computed as $(2/N)^{1/2}$. The data are a 10% representative sample of all non-zero lights in the radiance-calibrated data at the pixel level, where each pixel is $30 \times 30$ arc seconds.

# G An analytical top-coding correction

Researchers are often interested in aggregate measures, such as average luminosity or light inequality in a region or a country. Here we present simple formulas to correct these summary statistics for top-coding. These corrections work with arbitrary thresholds and Pareto shape parameters.

**Mean luminosity:** The top-coding corrected mean luminosity $\mu$ of a country or region is simply the weighted average of the bottom and top means $\mu_B$ and $\mu_T$. If the latter is the mean of a Pareto distribution starting at $y_c$, we have

$$\mu = \omega_B \mu_B + (1-\omega_B)\mu_T = \omega_B \mu_B + (1-\omega_B)\frac{\alpha}{\alpha-1} y_c \tag{G-1}$$

where $\omega_B$ and $\omega_T = 1-\omega_B$ are the shares of pixels below and above the threshold. A simple numerical illustration shows how correcting for top-coding drives up the mean luminosity. If top-coding starts at $y_c = 55$, affects 5% of the study area of interest, $\alpha$ is 1.5 and mean luminosity in the non-top-coded pixels is $\mu_B = 10$, then the corrected mean luminosity is 17.75 rather than 12.25.

**Spatial Gini coefficients:** The overall Gini coefficient can be written as the weighted sum of the bottom-share and top-share Ginis (i.e., the within-group Gini) as well as the difference between the top share of total lights minus the top share of pixels (i.e., the between-group Gini), such that

$$G = \omega_B \phi_B G_B + \omega_T \phi_T G_T + [\phi_T - \omega_T], \tag{G-2}$$

where the shares of all light accruing to the top and bottom groups are $\phi_B = \omega_B \mu_B / \mu$ and $\phi_T = \omega_T \mu_T / \mu$, and $G_T = 1/(2\alpha - 1)$. A greater share of top-coded pixels $\omega_T$, brighter top-coded pixels $\phi_T$, and a greater spread in the distribution of the top-coded data $G_T$ all increase the size of the correction.

The above decomposition of the Gini coefficient can be derived by defining the Gini coefficient over multiple groups as in Mookherjee and Shorrocks (1982)

$$G = \frac{1}{2N^2\mu} \sum_i \sum_j |y_i - y_j| \tag{G-3}$$

$$= \frac{1}{2N^2\mu} \sum_k \left( \sum_{i \in N_k} \sum_{j \in N_k} |y_i - y_j| + \sum_{i \in N_k} \sum_{j \notin N_k} |y_i - y_j| \right) \tag{G-4}$$

$$= \sum_k \left( \frac{N_k}{N} \right)^2 \frac{\mu_k}{\mu} G_k + \frac{1}{2N^2\mu} \sum_k \sum_{i \in N_k} \sum_{j \notin N_k} |y_i - y_j| \,. \tag{G-5}$$

where $G_K$ is the within group Gini coefficient of group $k$. The second term is a measure of group overlap including their between group differences.

Perfect separation (no overlap between groups) implies $\sum_{i \in N_k} \sum_{j \in N_h} |y_i - y_j| = N_k N_h |\mu_k - \mu_h|$. Hence, we can simplify equation eq. (G-5) to

$$G = \sum_k \left(\frac{N_k}{N}\right)^2 \frac{\mu_k}{\mu} G_k + \sum_k \sum_h \frac{N_k N_h}{2N^2 \mu} |\mu_k - \mu_h| \,. \tag{G-6}$$

With two bottom and top groups $k, h \in \{B, T\}$ (where $\mu_T > \mu_B$) and some algebra, this becomes

$$G = \left(\frac{N_B}{N}\right)^2 \frac{\mu_B}{\mu} G_B + \left(\frac{N_T}{N}\right)^2 \frac{\mu_T}{\mu} G_T + \left[\left(\frac{N_T}{N}\right)^2 \frac{\mu_T}{\mu} - \frac{N_T}{N}\right]. \tag{G-7}$$

Now define the pixel shares below and above the threshold as $\omega_B$ and $\omega_T$, where $\omega_T = 1 - \omega_B$ and the group's share of all income (light) as $\phi_B = \omega_B \frac{\mu_B}{\mu}$ and $\phi_T = \omega_T \frac{\mu_T}{\mu}$ to obtain eq. (G-2) above.

# H Characteristics of the corrected data

In this section we compare the back-on-the-envelop analytical corrections from the previous section with our corrected data at the pixel level, examine the correlations between our corrected data and the radiance calibrated data, and discuss the size of the top-coding correction around the world.

Figure H-1 illustrates the size of the correction in different countries with various scatter plots. As expected, the same characteristics that drive the number of top-coded pixels (see Section 2 in the paper) turn out to be predictive of the size of the correction in terms of country-wide mean luminosity and inequality in light. The correction is strongly increasing in GDP per capita, weakly in country size and moderately in population density. Numerous developing countries experience sizable corrections (such as Egypt, Paraguay or Mexico). City states, such as Singapore, have large top-coding corrections, as do smaller countries, like Israel and Estonia. Nevertheless, even large countries like the US experience a sizable increase in both mean luminosity (plus 7 DN) and the Gini coefficient (plus 14 percentage points). No single factor captures all the relevant heterogeneity.

Figure H-2 plots the time series graph of global inequality in lights from 1992 to 2013, both before and after the top-coding correction based on eq. (G-2). Parameter values of 1.4 and 1.6 serve as comparison bands for the benchmark case of 1.5. The global distribution of lights became slightly more unequal over the 1990s, remained flat in the first decade of the new millennium and then became temporarily more equal in the aftermath of the global financial crises and great recession. However, this year-to-year variation is completely swamped by the size of the top-coding correction.

Table H-1 reports mean luminosity and the Gini coefficient of inequality for 2010, using a wider range of parameters as robustness checks in the analytical correction in eq. (G-2). The parameters for this sensitivity analysis were chosen because of their equal distance to 1.5 rather than empirical relevance. Working with a smaller (larger) parameter than our benchmark $\alpha = 1.5$ implied more (less) inequality in the tail of the light distribution. The corrections are consequently larger (smaller). We can also see that parameter values of 1.4–1.6 only lead to very small differences in the magnitude of the correction. Also, using a higher $\alpha$ does not change the magnitude of the correction as much as using a smaller $\alpha$, as the comparison of the extreme values of 1.2 and 1.8 shows.

Table H-2 reports the mean luminosities and global Gini coefficients before and after the correction for each satellite, using both the analytic formulas and the data corrected at the pixel level. Our geo-referenced pixel-level replacement comes close to the analytic solutions but is generally more conservative (due to the fixed upper bound). Mean luminosity increases on average from 12.7 DN to 15.3–16.6 DN and inequality in lights from 0.47 to 0.56–0.59.

**Figure H-1** – Size of the correction and country characteristics

**(a)** Mean correction vs. GDP per capita

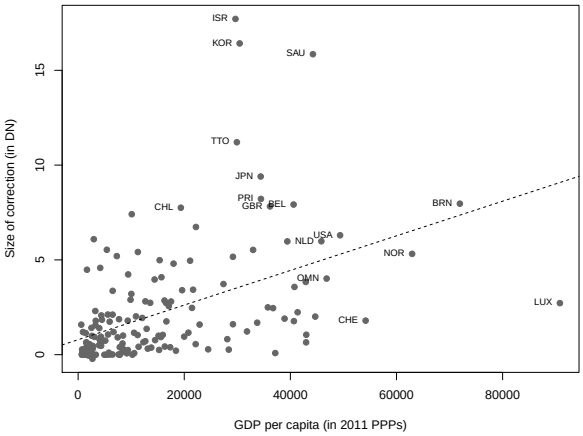


**(b)** Gini correction vs. GDP per capita

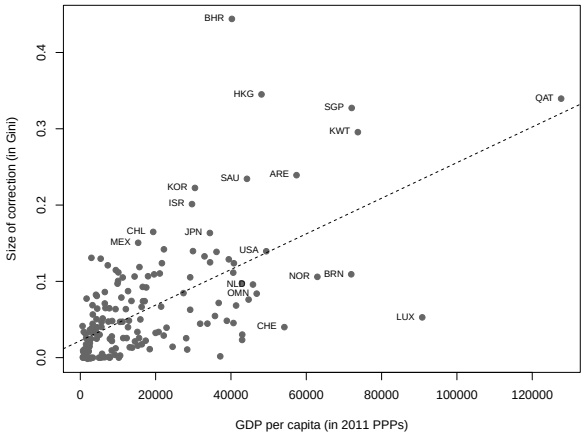


**(c)** Mean correction vs. log area

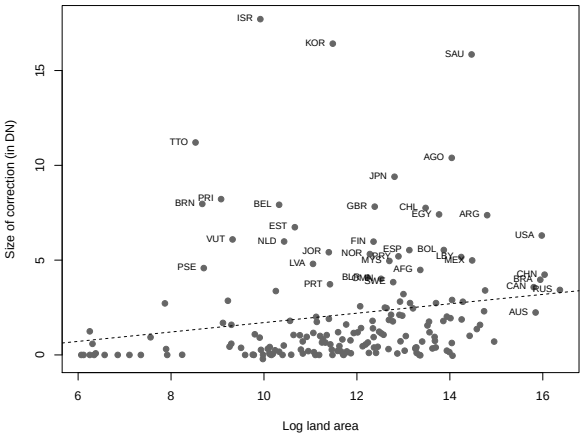


**(d)** Gini correction vs. log area

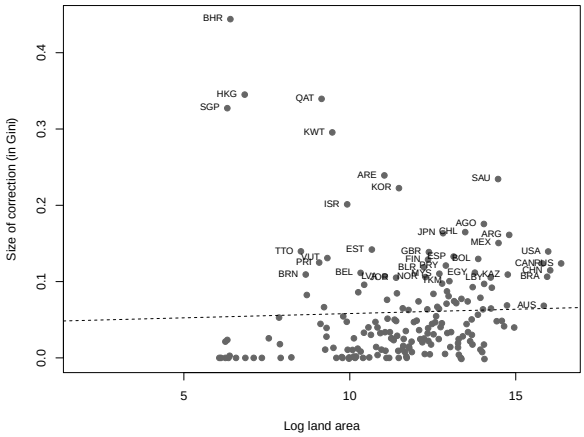


**(e)** Mean correction vs. log density

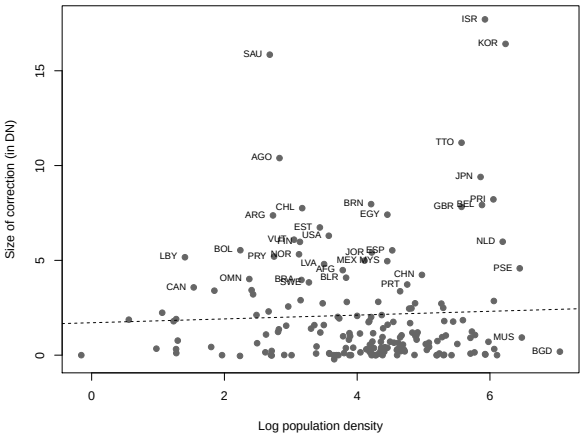


**(f)** Gini correction vs. log density

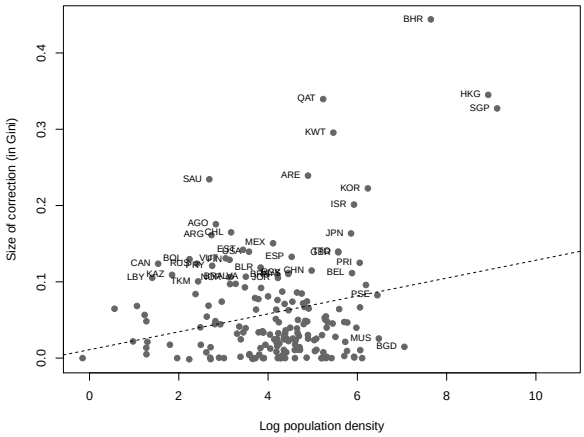


*Notes*: Illustration of how the correction of means and Gini coefficients, based on eq. (G-1) and eq. (G-2), correlate with log GDP per capita (PPP), log land area, and log population density. The data are a 10% representative sample of all non-zero lights in satellite F182010. GDP and population data are from the World Development Indicators. For display purposes, the left panels exclude countries with a correction of mean luminosity larger than 20 DN, these are Singapore, Hong Kong, Qatar, Bahrain, Kuwait, and the UAE. These countries are included in all panels on the right.

**Figure H-2** – Global Gini coefficient in lights before and after the correction

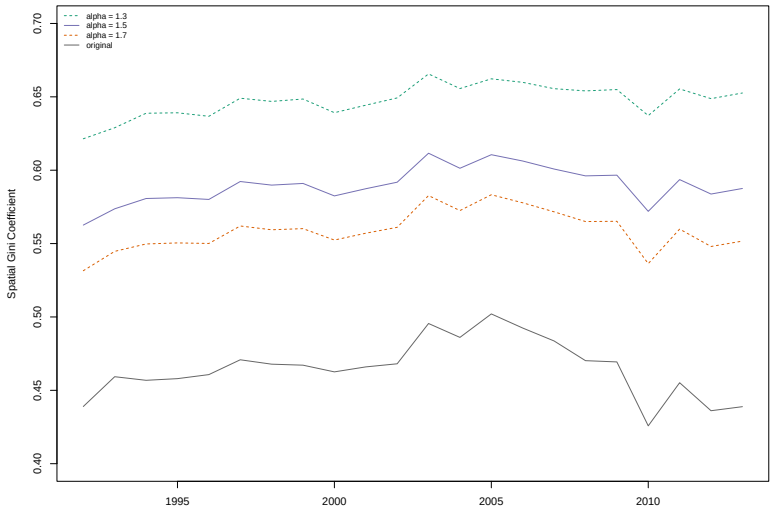


*Notes*: Illustration of the global top-coding correction. The figure shows global inequality in lights calculated by eq. (G-2) using the specified Pareto shape parameters. The input data are a representative 10% sample of non-zero lights. For years when more than two satellites flew concurrently, the values were averaged.

**Table H-1** – Correction of global mean and Gini coefficient in 2010, different parameters

| | Unadj. | *Pareto parameter* $\alpha =$ | | | | | | |
|---|---|---|---|---|---|---|---|---|
| | | 1.2 | 1.3 | 1.4 | **1.5** | 1.6 | 1.7 | 1.8 |
| Mean luminosity | 17.55 | 33.49 | 28.07 | 25.36 | 23.73 | 22.65 | 21.88 | 21.30 |
| Spatial Gini | 0.4258 | 0.6954 | 0.6372 | 0.5990 | 0.5720 | 0.5519 | 0.5363 | 0.5240 |
| Top share (light) | 0.2033 | 0.5825 | 0.5019 | 0.4487 | 0.4109 | 0.3828 | 0.3609 | 0.3435 |

*Notes*: The table computes the top-coding corrected mean and Gini coefficient of global inequality in lights for the year 2010 with different $\alpha$ parameters based on eq. (G-1) and eq. (G-2) with $y_c = 55$. The input data are a representative 10% sample of non-zero lights from satellite F18 in 2010.

**Table H-2** – Satellite level statistics of the top-coding correction

| Satellite | Top share (pixels) | *Top share (light)* Unadj | Adj | *Mean luminosity* Unadj | Form Adj | Pixel Adj | *Gini coefficient* Unadj | Form Adj | Pixel Adj |
|---|---|---|---|---|---|---|---|---|---|
| F101992 | 0.0381 | 0.1663 | 0.3096 | 13.83 | 17.81 | 16.70 | 0.4390 | 0.5626 | 0.5334 |
| F101993 | 0.0312 | 0.1568 | 0.2938 | 11.96 | 15.23 | 14.28 | 0.4593 | 0.5737 | 0.5456 |
| F101994 | 0.0349 | 0.1754 | 0.3207 | 12.02 | 15.67 | 14.60 | 0.4783 | 0.5980 | 0.5684 |
| F121994 | 0.0420 | 0.1733 | 0.3176 | 14.65 | 19.04 | 17.74 | 0.4353 | 0.5634 | 0.5316 |
| F121995 | 0.0376 | 0.1733 | 0.3174 | 13.09 | 17.02 | 15.85 | 0.4580 | 0.5813 | 0.5505 |
| F121996 | 0.0351 | 0.1670 | 0.3068 | 12.69 | 16.37 | 15.25 | 0.4607 | 0.5801 | 0.5494 |
| F121997 | 0.0394 | 0.1766 | 0.3210 | 13.45 | 17.57 | 16.31 | 0.4540 | 0.5799 | 0.5477 |
| F121998 | 0.0418 | 0.1816 | 0.3276 | 13.89 | 18.25 | 16.90 | 0.4474 | 0.5774 | 0.5436 |
| F121999 | 0.0467 | 0.1915 | 0.3412 | 14.74 | 19.62 | 18.08 | 0.4447 | 0.5802 | 0.5449 |
| F141997 | 0.0316 | 0.1739 | 0.3169 | 10.98 | 14.29 | 13.28 | 0.4876 | 0.6047 | 0.5747 |
| F141998 | 0.0305 | 0.1680 | 0.3067 | 10.94 | 14.13 | 13.13 | 0.4883 | 0.6023 | 0.5720 |
| F141999 | 0.0278 | 0.1648 | 0.3011 | 10.15 | 13.06 | 12.13 | 0.4895 | 0.6017 | 0.5714 |
| F142000 | 0.0318 | 0.1689 | 0.3062 | 11.34 | 14.67 | 13.59 | 0.4852 | 0.6003 | 0.5687 |
| F142001 | 0.0350 | 0.1817 | 0.3276 | 11.64 | 15.30 | 14.16 | 0.4856 | 0.6069 | 0.5754 |
| F142002 | 0.0377 | 0.1872 | 0.3375 | 12.14 | 16.08 | 14.90 | 0.4896 | 0.6126 | 0.5818 |
| F142003 | 0.0382 | 0.1930 | 0.3409 | 11.96 | 15.96 | 14.65 | 0.4928 | 0.6177 | 0.5836 |
| F152000 | 0.0370 | 0.1685 | 0.3063 | 13.25 | 17.13 | 15.89 | 0.4399 | 0.5647 | 0.5308 |
| F152001 | 0.0354 | 0.1645 | 0.3011 | 12.93 | 16.64 | 15.46 | 0.4463 | 0.5679 | 0.5351 |
| F152002 | 0.0372 | 0.1700 | 0.3085 | 13.18 | 17.08 | 15.82 | 0.4465 | 0.5710 | 0.5370 |
| F152003 | 0.0270 | 0.1582 | 0.2894 | 10.28 | 13.11 | 12.17 | 0.4982 | 0.6055 | 0.5751 |
| F152004 | 0.0276 | 0.1642 | 0.2979 | 10.08 | 12.97 | 12.00 | 0.5080 | 0.6163 | 0.5853 |
| F152005 | 0.0279 | 0.1604 | 0.2953 | 10.44 | 13.36 | 12.43 | 0.5115 | 0.6171 | 0.5886 |
| F152006 | 0.0293 | 0.1666 | 0.2988 | 10.56 | 13.63 | 12.55 | 0.5135 | 0.6217 | 0.5892 |
| F152007 | 0.0279 | 0.1547 | 0.2844 | 10.74 | 13.68 | 12.69 | 0.5049 | 0.6099 | 0.5795 |
| F162004 | 0.0340 | 0.1734 | 0.3129 | 11.82 | 15.38 | 14.23 | 0.4641 | 0.5863 | 0.5528 |
| F162005 | 0.0285 | 0.1642 | 0.2993 | 10.44 | 13.43 | 12.46 | 0.4926 | 0.6040 | 0.5732 |
| F162006 | 0.0348 | 0.1707 | 0.3041 | 12.26 | 15.91 | 14.61 | 0.4714 | 0.5908 | 0.5546 |
| F162007 | 0.0403 | 0.1861 | 0.3302 | 13.05 | 17.28 | 15.86 | 0.4624 | 0.5916 | 0.5554 |
| F162008 | 0.0395 | 0.1832 | 0.3285 | 12.97 | 17.11 | 15.78 | 0.4702 | 0.5961 | 0.5622 |
| F162009 | 0.0417 | 0.1862 | 0.3356 | 13.50 | 17.87 | 16.54 | 0.4694 | 0.5966 | 0.5644 |
| F182010 | 0.0591 | 0.2033 | 0.3614 | 17.55 | 23.73 | 21.89 | 0.4258 | 0.5720 | 0.5361 |
| F182011 | 0.0494 | 0.2020 | 0.3595 | 14.78 | 19.95 | 18.41 | 0.4552 | 0.5936 | 0.5598 |
| F182012 | 0.0576 | 0.2118 | 0.3734 | 16.44 | 22.45 | 20.68 | 0.4361 | 0.5838 | 0.5481 |
| F182013 | 0.0578 | 0.2151 | 0.3800 | 16.23 | 22.28 | 20.55 | 0.4389 | 0.5876 | 0.5530 |
| **Average** | **0.0374** | **0.1765** | **0.3194** | **12.65** | **16.56** | **15.34** | **0.4691** | **0.5917** | **0.5595** |

*Notes*: The table reports summary statistics of the global lights data before the top-coding correction and after the analytical, formula-based correction at the aggregate level (eq. (G-1) and eq. (G-2)) as well as the pixel-level correction from the paper. Column 1 reports the share of pixels above 55 DN, Column 2 and 3 the share of lights emitted by these top pixels respectively in the unadjusted and adjusted data set. Columns 4-6 and 7-9 report the mean luminosity and Gini coefficient, respectively for the unadjusted data, the analytical, formula-based correction and the pixel-level corrected data. All corrections use $\alpha = 1.5$ and $y_c = 55$ for the Pareto tail.

# I Benchmarking exercises

## I.1 Light-output elasticities at the national level

To validate our corrected data, we estimate light-output elasticities at the national level in the spirit of Henderson et al. (2012). Henderson et al. (2012) focus on the predictive relationship, that is, how lights predict changes in GDP, by running fixed effects regressions of log GDP on log lights per square kilometer. They report an elasticity income with respect to lights around 0.28. We then also examine the structural relationship where lights are on the left hand side and GDP on the right hand side (as in Chen and Nordhaus, 2011, Hu and Yao, 2019). Hu and Yao (2019) recently showed that there is significant non-linearity in the light production function which could be related to top-coding, as it appears to be weaker in the new VIIRS data (which is not top-coded). We replicate these results using a matched sample of the stable lights data, our top-coding corrected lights and the radiance-calibrated data for the seven years which all three data sources have in common over the period from 1996 to 2010. Note that both ways of estimating the relationship delivers biased estimates that depend differently on measurement errors in GDP and lights, and we make no attempt to correct for these biases here.

Table I-1 reports the estimates of the predictive relationship and shows that—even at the highly aggregated country level—our top-coding correction leads to marginal improvements. The corrected data always yield the highest within-$R^2$ and marginally larger estimates. When including quadratic terms on the right hand side, their estimated coefficients are smallest for the corrected and radiance-calibrated data. This suggests that top-coding plays some small role in the non-linearity of the predictive relationship.

Table I-2 turns things around and focuses on what is generally considered the structural relationship, that is, how lights react to changes in GDP. Here, too, we obtain the highest elasticity when we consider the corrected data and, by definition, exactly the same $R^2$ as in the reverse regression. In line with Hu and Yao (2019), we find evidence suggesting that there is non-linearity in the light production function. While it is weaker in the corrected data, it does not appear to qualitatively differ across the three data sources. Of course, these estimates are subject to measurement errors in GDP.

In summary, the results are not materially different at the national level, so that for an analysis of the light-output relationship at such a high level of aggregation either data can be used without explicitly considering the role of top-coding. Note that it is not clear whether we should expect the corrected data to deliver regression coefficients which are closer to the radiance-calibrated data. The spectral mixing process of Hsu et al. (2015) created a lot of noise in areas which are not top-coded and provide the overwhelming share of the variation analyzed by these regressions, so it is not implausible that our corrected data delivers the strongest results.

**Table I-1** – Light-output elasticity, country-level, 1996–2010

| | *Dependent variable: GDP in 2005 PPPs* | | | | | |
|---|---|---|---|---|---|---|
| | (1) Stable | (2) Corrected | (3) Radiance | (4) Stable | (5) Corrected | (6) Radiance |
| $\ln \text{LIGHTS}_{it}$ | 0.275*** | 0.278*** | 0.233*** | 0.193*** | 0.221*** | 0.182*** |
| | (0.067) | (0.064) | (0.054) | (0.047) | (0.046) | (0.034) |
| $(\ln \text{LIGHTS}_{it})^2$ | | | | -0.020*** | -0.015** | -0.017* |
| | | | | (0.007) | (0.006) | (0.010) |
| Country FE | ✓ | ✓ | ✓ | ✓ | ✓ | ✓ |
| Year FE | ✓ | ✓ | ✓ | ✓ | ✓ | ✓ |
| Within-$R^2$ | 0.172 | 0.184 | 0.147 | 0.202 | 0.207 | 0.170 |
| Observations | 1288 | 1288 | 1288 | 1288 | 1288 | 1288 |
| Countries | 186 | 186 | 186 | 186 | 186 | 186 |

*Note(s)*: The table reports panel FE estimates of the predictive relationship between light intensity and GDP within countries. $\ln \text{LIGHTS}_{it}$ are defined as the log average light intensity per sq. km. $\ln GDP_{it}$ is the log of GDP in 2005 PPPs from the World Development Indicators. The specifications are variants of $\ln \text{GDP}_{it} = \beta \ln \text{LIGHTS}_{it} + \gamma(\ln \text{LIGHTS}_{it})^2 + c_i + s_t + \epsilon_{it}$ where $c_i$ is a country fixed effect, and $s_t$ are year dummies. Country-clustered standard errors are provided in parentheses. Significant at: * $p < 0.10$, ** $p < 0.05$, *** $p < 0.01$.

**Table I-2** – Light production function, country-level, 1996–2010

| | *Dependent variable: Log lights per sq. km* | | | | | |
|---|---|---|---|---|---|---|
| | (1) Stable | (2) Corrected | (3) Radiance | (4) Stable | (5) Corrected | (6) Radiance |
| $\ln \text{GDP}_{it}$ | 0.628*** | 0.663*** | 0.632*** | 0.586*** | 0.627*** | 0.589*** |
| | (0.101) | (0.093) | (0.076) | (0.080) | (0.077) | (0.073) |
| $(\ln \text{GDP}_{it})^2$ | | | | -0.037*** | -0.032*** | -0.038*** |
| | | | | (0.010) | (0.010) | (0.010) |
| Country FE | ✓ | ✓ | ✓ | ✓ | ✓ | ✓ |
| Year FE | ✓ | ✓ | ✓ | ✓ | ✓ | ✓ |
| Within-$R^2$ | 0.172 | 0.184 | 0.147 | 0.200 | 0.204 | 0.172 |
| Observations | 1288 | 1288 | 1288 | 1288 | 1288 | 1288 |
| Countries | 186 | 186 | 186 | 186 | 186 | 186 |

*Note(s)*: The table reports panel FE estimates of the light production function within countries. $\ln \text{LIGHTS}_{it}$ are defined as the log average light intensity per sq. km. $\ln GDP_{it}$ is the log of GDP in 2005 PPPs from the World Development Indicators. The specifications are variants of $\ln Lights_{it} = \beta \ln \text{GDP}_{it} + \gamma(\ln \text{GDP}_{it})^2 + c_i + s_t + \epsilon_{it}$ where $c_i$ is a country fixed effect, and $s_t$ are year dummies. Country-clustered standard errors are provided in parentheses. Significant at: * $p < 0.10$, ** $p < 0.05$, *** $p < 0.01$.

## I.2 Light-output elasticities at the subnational level

Lights are particularly useful as a proxy for economic activity at the regional level or other smaller geographies. This is precisely where the influence of top-coding will be more pronounced. We now study how top-coding affects the non-linearity of the estimated light production function (in the spirit of Hu and Yao, 2019) in U.S. counties and German districts. Both countries publish subnational accounts data of the highest quality, which minimizes the attenuation bias caused by measurement errors in GDP and allows us to directly study variation in the structural parameter of interest. While some developing countries publish similar data, they are likely to include sizable errors in the estimation of regional GDP, severely limiting what we can learn from them without addressing these biases.

Figure I-1 plots the raw data for 401 German districts (*Kreise*) from 2000 to 2013 and 3,080 U.S. counties from 2001 to 2013. It visualizes how much the top-coding correction changes the light-output relationship in regions that are moderately to very economically dense. Our correction appears to restore linearity at the top in Germany, while it appears to shift up the point at which the relationship starts to deviate from a line in the case of U.S. counties.

Figure I-2 plots the average light intensity per square kilometer indicated by both data sources over population density in German districts and U.S. counties. It illustrates that there is a similar quadratic relationship as in the light production function estimated above, which again disappears or becomes substantially weaker in the corrected data. As top-coding occurs primarily in dense urban areas, we take this as evidence that the stable lights data artificially create non-linearity in comparatively dense regions.

Table I-3 estimates the light production function for the German districts. We present two-way fixed effects estimates (columns 1 and 2), pooled estimates with year fixed effects (columns 3 and 4), and cross-sectional estimates (columns 5 and 6). In each case, we compare the estimates obtained for a quadratic in log GDP (per sq. km) for the stable lights and corrected data. The data are centered so that GDP and lights are zero at their sample averages. All columns using the stable lights data suggest that there is substantial non-linearity in the light production function, with decreasing elasticities of light w.r.t. income as economic density increases. We little evidence in favor of a negative and significant quadratic term when using the top-coding corrected data, no matter if we estimate this using only within district or also with between district variation. This suggests that top-coding seems to be driving a substantial portion of this non-linearity at the district level in Germany.

Table I-4 shows similar estimates for U.S. counties. Here, too, we find some evidence that the light production function is non-linear in economic density. As before, the estimates of the squared terms are negative and significant at the 10%-level or smaller

whenever the stable lights data are used. However, the non-linearity disappears when we consider changes in nighttime lights within counties and becomes considerably weaker (falls by 40%) when we also use between-county variation. Given that measurement errors in GDP should be small in this context and are likely to be unrelated to measurement errors in lights, we take this as additional evidence that top-coding creates artificial non-linearity at high economic densities by limiting how much the brightness of these regions can grow.

**Figure I-1** – Non-linearity of light production function in Germany and USA

**(a)** Germany – Stable

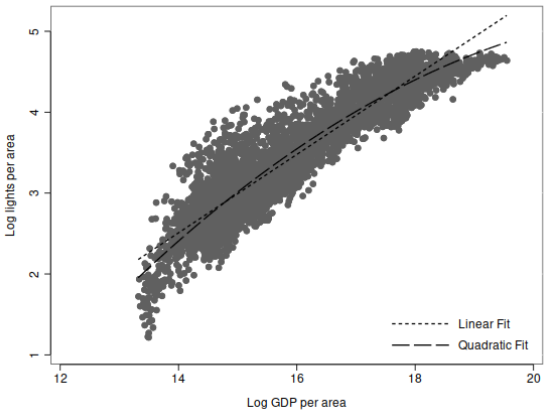


**(b)** Germany – Corrected

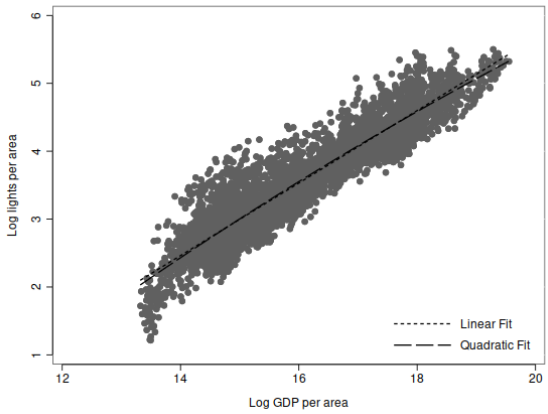


**(c)** USA – Stable

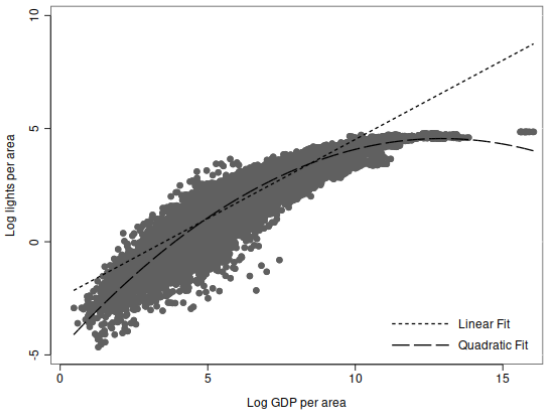


**(d)** USA – Corrected

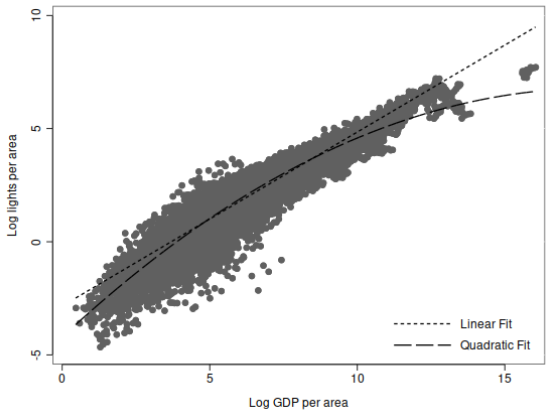


*Notes*: Illustration of the light-output relationship in German districts and U.S. counties. All panels show the log of average light intensity per sq. km. against the log of GDP per sq. km., including a linear and a quadratic fit. Panel (a) uses the stable lights data in German districts as the dependent variable. Panel (b) uses our corrected data in German districts as the dependent variable. Panel (c) uses the stable lights data in U.S. counties as the dependent variable. Panel (d) uses our corrected data in U.S. counties as the dependent variable.

**Figure I-2** – Light density and population density in Germany and USA

**(a)** Germany – Stable

**(b)** Germany – Corrected

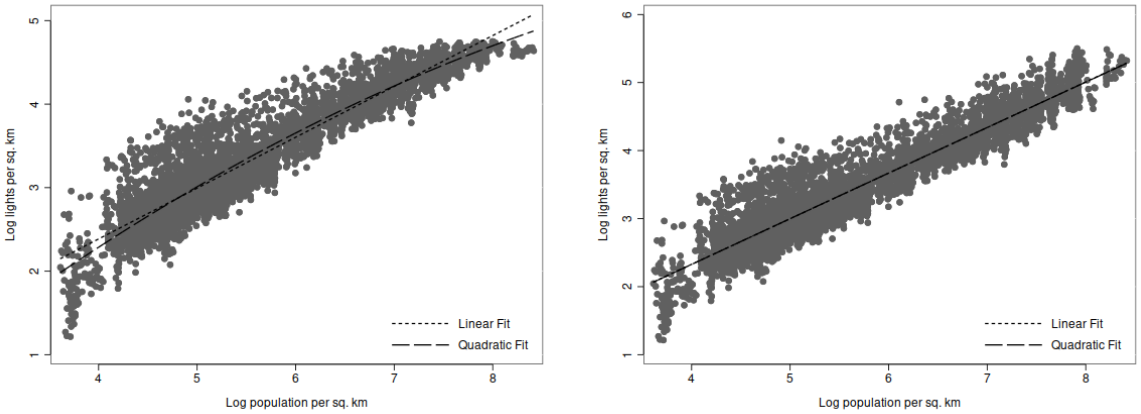


**(c)** USA – Stable

**(d)** USA – Corrected

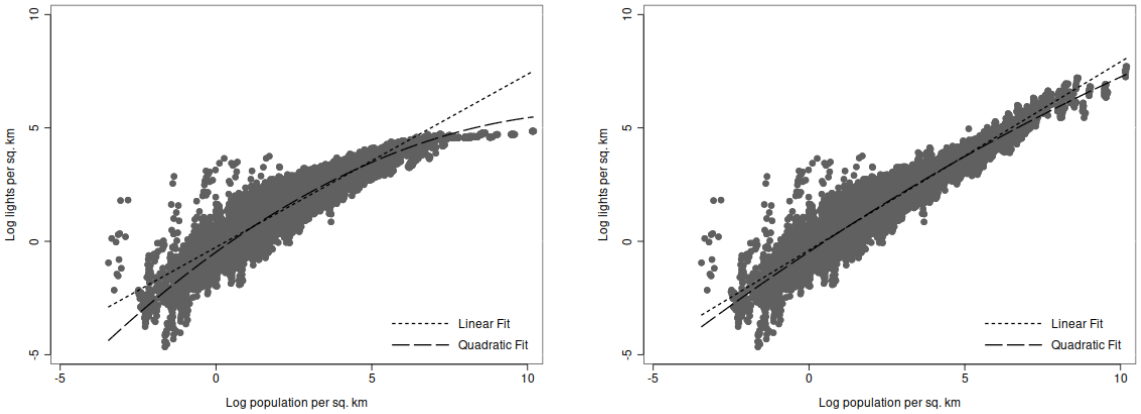


*Notes*: Illustration of the light-population relationship in German districts and U.S. counties. All panels show the log of average light intensity per sq. km. against the log of population density (population per sq. km.), including a linear and a quadratic fit. Panel (a) uses the stable lights data in German districts as the dependent variable. Panel (b) uses our corrected data in German districts as the dependent variable. Panel (c) uses the stable lights data in U.S. counties as the dependent variable. Panel (d) uses our corrected data in U.S. counties as the dependent variable.

**Table I-3** – Estimated light production function, Germany at district level, 2000–2013

| | *Dependent variable: Log lights per sq. km* | | | | | |
|---|---|---|---|---|---|---|
| | *Panel* | | *Pooled* | | *Cross-section* | |
| | (1) | (2) | (3) | (4) | (5) | (6) |
| | Stable | Corrected | Stable | Corrected | Stable | Corrected |
| $\ln \text{GDP}_{it}$ | 0.222*** | 0.172*** | 0.510*** | 0.539*** | 0.502*** | 0.534*** |
| | (0.034) | (0.029) | (0.008) | (0.009) | (0.009) | (0.010) |
| $(\ln \text{GDP}_{it})^2$ | -0.076*** | -0.005 | -0.034*** | -0.009* | -0.033*** | -0.009 |
| | (0.005) | (0.006) | (0.005) | (0.006) | (0.005) | (0.006) |
| Time FE | ✓ | ✓ | ✓ | ✓ | – | – |
| District FE | ✓ | ✓ | – | – | – | – |
| Within-$R^2$ | 0.0671 | 0.00950 | 0.916 | 0.922 | 0.930 | 0.932 |
| Observations | 5614 | 5614 | 5614 | 5614 | 401 | 401 |
| Districts | 401 | 401 | 401 | 401 | 401 | 401 |

*Notes*: The table reports panel FE estimates of the light production function within and across German districts (Kreise). $\ln \text{LIGHTS}_{it}$ are defined as the log average light intensity per sq. km. $\ln GDP_{it}$ is the log of GDP per sq. km in current LCU from the GENESIS regional database. The specifications are variants of $\ln \text{LIGHTS}_{it} = \beta \ln \text{GDP}_{it} + \gamma(\ln \text{GDP}_{it})^2 + c_i + s_t + \epsilon_{it}$ where $c_i$ is a district fixed effect, and $s_t$ are year dummies. The cross-sectional regressions do not include any fixed effects. District-clustered standard errors are provided in parentheses. Significant at: * $p < 0.10$, ** $p < 0.05$, *** $p < 0.01$.

**Table I-4** – Estimated light production function, USA at county level, 2001–2013

| | *Dependent variable: Log lights per sq. km* | | | | | |
|---|---|---|---|---|---|---|
| | *Panel* | | *Pooled* | | *Cross-section* | |
| | (1) | (2) | (3) | (4) | (5) | (6) |
| | Stable | Corrected | Stable | Corrected | Stable | Corrected |
| $\ln \text{GDP}_{it}$ | 0.375*** | 0.396*** | 0.750*** | 0.801*** | 0.751*** | 0.803*** |
| | (0.039) | (0.038) | (0.005) | (0.005) | (0.005) | (0.005) |
| $(\ln \text{GDP}_{it})^2$ | -0.006* | 0.001 | -0.056*** | -0.034*** | -0.058*** | -0.035*** |
| | (0.004) | (0.004) | (0.001) | (0.002) | (0.002) | (0.002) |
| Time FE | ✓ | ✓ | ✓ | ✓ | – | – |
| County FE | ✓ | ✓ | – | – | – | – |
| Within-$R^2$ | 0.118 | 0.118 | 0.882 | 0.895 | 0.891 | 0.903 |
| Observations | 40039 | 40039 | 40039 | 40039 | 3080 | 3080 |
| Counties | 3080 | 3080 | 3080 | 3080 | 3080 | 3080 |

*Notes*: The table reports panel FE estimates of the light production function within and across U.S. counties. $\ln \text{LIGHTS}_{it}$ are defined as the log average light intensity per sq. km. $\ln GDP_{it}$ is the log of GDP per sq. km in current LCU from the Bureau of Economic Analysis (BEA) regional database (CAGDP1). The specifications are variants of $\ln \text{LIGHTS}_{it} = \beta \ln \text{GDP}_{it} + \gamma(\ln \text{GDP}_{it})^2 + c_i + s_t + \epsilon_{it}$ where $c_i$ is a district fixed effect, and $s_t$ are year dummies. The cross-sectional regressions do not include any fixed effects. District-clustered standard errors are provided in parentheses. Significant at: * $p < 0.10$, ** $p < 0.05$, *** $p < 0.01$.

## I.3 Light-wealth elasticities across cities within African countries

Lights are often used as a replacement for survey data on income and wealth at small geographies, when such survey data are unavailable or not widely available. Here we investigate whether top-coding makes a difference in the mapping of light to household wealth across African cities. As before, we are particularly interested in whether the relationship appears to be linear above the top-coding threshold or whether we observe a change in the relevant estimates. To this end, we use DHS survey data for urban sampling clusters in 29 African countries over the period from 1992 to 2013. Bruederle and Hodler (2018) compile this data to study correlations between various measures of household welfare and nighttime lights. Their primary measure is the DHS wealth index, which groups households in five groups according to scores derived from a principal component analysis of asset ownership. Bruederle and Hodler (2018) report a semi-elasticity of wealth to lights around 0.27.

Table I-5 reports estimates of the wealth-lights relationship across (up to) 7,601 urban survey clusters in 29 African countries. We present models that use within-country, within-country-year, and within-province-year variation to study how increases in the stable lights and corrected data translate into changes in the DHS wealth index. As survey locations change from survey to survey, we cannot exclusively use within-location variation but have to compare across locations within some geography (and year). In all panels, we allow the elasticity of wealth with respect to light to change for top-coded clusters. Since clusters consist of several pixels, we use the difference between the corrected light intensity and stable light intensity to identify top-coded clusters of varying severity. Following Michalopoulos and Papaioannou (2013), we always control for population density. This eliminates some of the comparability problems between household wealth and light emissions in the larger cluster. However, we cannot convert lights into a per household quantity without knowing the exact location and light emitted by the sampled household(s).

The results show that the wealth to light elasticity becomes very unstable in top-coded clusters when the stable lights data are used. In every specification, we find that the elasticity above the threshold is a multiple of the elasticity below the threshold and appears to increase in the threshold. This suggests that the variation in lights is limited above the threshold—recall that top-coding is now a matter of degree—although there is lots of variation in household wealth, so that small differences in average light intensities translate into large changes in household wealth. The results using the corrected data suggest that there is no such discontinuity for top-coded clusters. Instead, our estimates suggest that the relationship is linear in log lights, especially when we consider more severely top-coded clusters with a difference of at least 10 DN per sq. km. across both

data sources. Moreover, the within-$R^2$ is always moderately larger when the corrected data are used. Our results are similar whether we control for population density or not (not reported).

**Table I-5** – Light-wealth relationship, urban DHS survey clusters, 1992–2013

| | *Dependent variable: DHS wealth index* | | | | | |
|---|---|---|---|---|---|---|
| | (1) | (2) | (3) | (4) | (5) | (6) |
| | Stable lights | | | Corrected lights | | |
| | *Panel a) Top-coded urban clusters when $\Delta DN_{it} > 0$* | | | | | |
| $\ln$ Lights$_{ct}$ | 0.219*** | 0.221*** | 0.225*** | 0.230*** | 0.232*** | 0.230*** |
| | (0.027) | (0.027) | (0.022) | (0.028) | (0.028) | (0.023) |
| $\ln$ Lights$_{ct}$ × Top-coded$_{ct}$ | 0.492** | 0.485** | 0.394 | 0.054** | 0.053** | 0.064** |
| | (0.225) | (0.228) | (0.232) | (0.024) | (0.025) | (0.031) |
| Within-$R^2$ | 0.261 | 0.263 | 0.177 | 0.275 | 0.278 | 0.187 |
| | *Panel b) Top-coded urban clusters when $\Delta DN_{it} > 10$* | | | | | |
| $\ln$ Lights$_{ct}$ | 0.230*** | 0.232*** | 0.236*** | 0.232*** | 0.234*** | 0.237*** |
| | (0.026) | (0.026) | (0.023) | (0.027) | (0.027) | (0.024) |
| $\ln$ Lights$_{ct}$ × Top-coded$_{ct}$ | 1.683*** | 1.708*** | 1.957*** | -0.002 | -0.003 | 0.008 |
| | (0.205) | (0.209) | (0.349) | (0.032) | (0.032) | (0.038) |
| Within-$R^2$ | 0.273 | 0.276 | 0.187 | 0.277 | 0.280 | 0.187 |
| | *Panel c) Top-coded urban clusters when $\Delta DN_{it} > 20$* | | | | | |
| $\ln$ Lights$_{it}$ | 0.233*** | 0.235*** | 0.238*** | 0.234*** | 0.236*** | 0.238*** |
| | (0.026) | (0.027) | (0.023) | (0.027) | (0.027) | (0.025) |
| $\ln$ Lights$_{it}$ × Top-coded$_{it}$ | 1.593*** | 1.610*** | 1.964*** | -0.043 | -0.044 | -0.028 |
| | (0.439) | (0.442) | (0.458) | (0.037) | (0.036) | (0.041) |
| Within-$R^2$ | 0.276 | 0.279 | 0.186 | 0.278 | 0.281 | 0.187 |
| Pop. density | ✓ | ✓ | ✓ | ✓ | ✓ | ✓ |
| Country & Year FE | ✓ | – | – | ✓ | – | – |
| Country-Year FE | – | ✓ | – | – | ✓ | – |
| Province-Year FE | – | – | ✓ | – | – | ✓ |
| Observations | 7601 | 7601 | 7405 | 7601 | 7601 | 7405 |
| Countries | 29 | 29 | 29 | 29 | 29 | 29 |

*Note(s)*: The table reports regression estimates of the relationship between DHS wealth and light intensity within 2 km of urban DHS sampling clusters. $\ln$ Lights$_{it}$ are defined as the log average light intensity per sq. km. in a survey cluster using either the stable lights or corrected lights data. $\Delta DN_{it}$ is the difference between the corrected lights and stable lights per sq. km. in the cluster, so that positive values indicate the intensity of top-coding in the entire cluster. DHS$_{it}$ is the average DHS wealth index in a survey cluster from Bruederle and Hodler (2018). The specifications are variants of DHS$_{it} = \beta \ln$ Lights$_{it} + \gamma \ln$ Lights$_{it}$ × Top-coded$_{it} + \theta \ln$ Pop. Dens. $+ c_i + s_t + \epsilon_{it}$ where Top-coded$_{it} \equiv \mathbb{I}(\Delta DN_{it} > k)$ and $k$ is a constant defined in the panel header, $c_i$ is a country fixed effect, and $s_t$ are year dummies. Country-clustered standard errors are provided in parentheses. Significant at: * $p < 0.10$, ** $p < 0.05$, *** $p < 0.01$.

# J Additional results for African cities

## J.1 City growth in sub-Saharan Africa

Here we present additional results for the application of our correction to city growth in sub-Saharan Africa.

Figure J-1 shows the urban extents of selected cities and compares them with Google Earth images at the end of the periods we use to delineate urban areas, i.e., 12/1994 and 12/2013. The urban footprint detected by our algorithm coincides well with built-up structures (see Abrahams et al., 2018, for a more systematic comparison).

Figure J-2 compares the sum of lights in each of the three data series (stable lights, corrected data, radiance-calibrated data) for the available years. The radiance-calibrated data exhibit large fluctuations and jumps over time. On the other hand, the time series of the stable lights and corrected data fluctuate less and indicate a positive trend over the entire period.

Table J-1 reports descriptive statistics using only the years from 1996 to 2010, making the results comparable to the radiance-calibrated data. The stable lights data indicate similar growth rates for primary and secondary cities, just as in the longer sample. However, the corrected and radiance-calibrated lights suggest that primary cities grew faster at the intensive margin. The radiance-calibrated lights even indicate a negative average growth rate for secondary cities, which might be related to their large annual fluctuations. We observe positive growth in secondary cities for the corrected lights, but lower than that of primary cities.

Table J-2 gives an overview of the countries included in our study. The table reports the names of the primary city, the number of secondary cities, and the annualized growth rates for the stable lights and corrected data at the intensive margin. The corrections are larger in primate than in each country's secondary cities.

Table J-3 varies the minimum city size to account for the uncertainty in classifying cities as secondary. We focus on the strictest specification with country-year fixed effects. The main results are robust to larger thresholds and even increase when secondary cities are defined as fewer, larger cities. However, including smaller settlements increases noise, as their light intensity represents fewer and fewer data points per year, generating large jumps in their light intensity.

Table J-4 shows that our results are robust to excluding each of the African regions in turn. Using the corrected data, we reject the null that the interaction of the linear trend and the primacy dummy is zero in almost all regions. When we exclude East Africa, the coefficient marginally loses significance. Still, it remains within a standard error of the main result, while the stable lights data suggest that primate cities grow slower in this region.

**Figure J-1** – Urban extents of selected cities

**(a)** Lagos, 12/1994

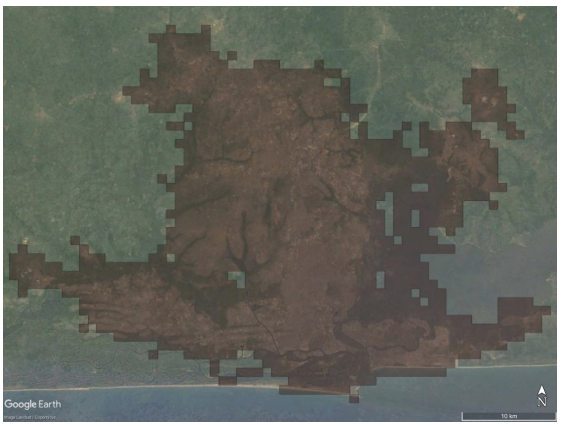


**(b)** Lagos, 12/2013

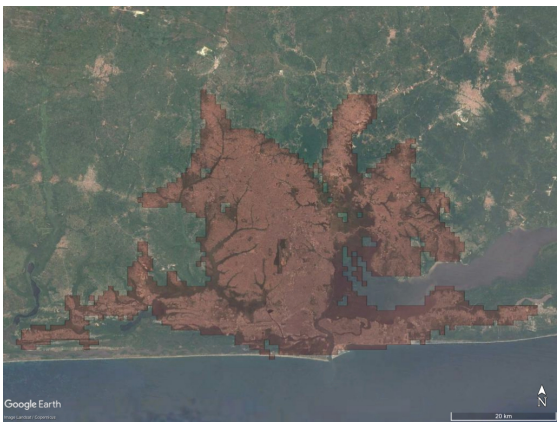


**(c)** Luanda, 12/1994


**(d)** Luanda, 12/2013


**(e)** Johannesburg, 12/1994

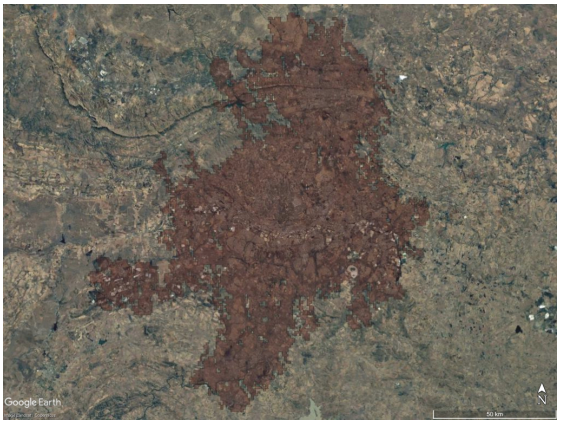


**(f)** Johannesburg, 12/2013


*Notes*: Illustration of the urban extents detection algorithm presented in the text. Note the differences in map scale. Comparison of 1992-1994 urban footprint with December 1994 and December 2013 Landsat/ Copernicus images obtained via Google Earth Pro. Google Earth images are used as part of their "fair use" policy. All rights to the underlying maps belong to Google.

**Figure J-2** – Trends in light emitted by African cities, initial boundaries

**(a)** Primary cities

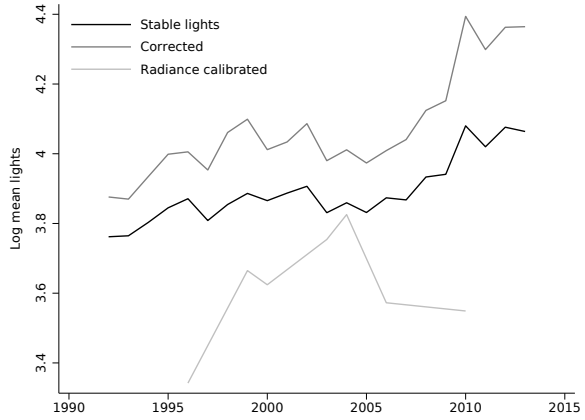


**(b)** Secondary cities

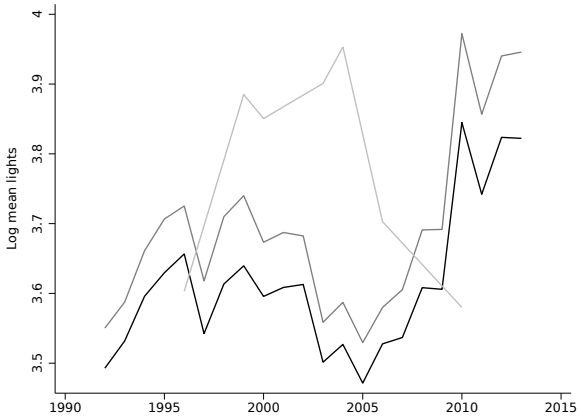


*Notes*: The figure illustrates the average light intensity over time in the sample of African cities (within the initial boundaries).

**Table J-1** – Summary statistics for African cities, 1996–2010, envelopes and initial boundaries

| | *Stable Lights* | | *Corrected Lights* | | *Radcal Lights* | |
|---|---|---|---|---|---|---|
| | Primate | Secondary | Primate | Secondary | Primate | Secondary |
| | *Panel a) Sum of lights in envelopes* | | | | | |
| Sum in 1996 | 25227.59 | 2407.13 | 28488.13 | 2556.14 | 37816.48 | 2831.96 |
| | (77801.08) | (7679.08) | (92532.01) | (9001.96) | (131460.00) | (12535.54) |
| Sum in 2010 | 35810.66 | 3169.00 | 46449.94 | 3515.06 | 46636.69 | 2934.17 |
| | (98116.36) | (9094.25) | (135162.59) | (12027.36) | (144064.49) | (12468.45) |
| Annualized growth rate | 0.0250 | 0.0196 | 0.0349 | 0.0228 | 0.0150 | 0.0025 |
| | *Panel b) Sum of lights in initial boundaries* | | | | | |
| Sum in 1996 | 22665.46 | 2095.41 | 25926.01 | 2244.42 | 13356.53 | 1986.41 |
| | (73810.12) | (7378.00) | (88538.22) | (8720.04) | (20672.99) | (6679.74) |
| Sum in 2010 | 27934.93 | 2529.58 | 38238.95 | 2873.30 | 16425.64 | 1940.90 |
| | (88793.92) | (8430.63) | (125218.42) | (11441.46) | (24210.20) | (6697.16) |
| Annualized growth rate | 0.0149 | 0.0135 | 0.0278 | 0.0176 | 0.0148 | -0.0017 |

*Notes*: The table reports a selection of summary statistics for African cities based on their envelopes (panel A) and their initial boundaries (panel B). In contrast to Table 3, the time period is from 1996 to 2010 to match the availability of the radiance-calibrated lights. Standard deviations in parentheses. Annualized growth rates are computed as $\frac{1}{14}(\ln x_{2010} - \ln x_{1996})$, where $x$ refers to the data per group reported in the table.

**Table J-2** – Annualized growth rates of cities in Africa, 1992–2013, intensive margin

| Primate city | Primate city growth: Stable lights | Corrected | Secondary cities | Secondary city growth: Stable lights | Corrected | Country |
|---|---|---|---|---|---|---|
| Luanda | 0.0282 | 0.0834 | 5 | 0.2034 | 0.2115 | Angola |
| Bujumbura | 0.0291 | 0.0317 | 3 | 0.1827 | 0.1823 | Burundi |
| Cotonou | 0.0328 | 0.0406 | 10 | 0.1775 | 0.1776 | Benin |
| Ouagadougou | 0.0265 | 0.0325 | 4 | 0.1842 | 0.1846 | Burkina Faso |
| Gaborone | 0.0114 | 0.0123 | 0 | | | Botswana |
| Bangui | 0.0193 | 0.0250 | 8 | 0.1642 | 0.1671 | Central African Rep. |
| Abidjan | -0.0076 | -0.0076 | 0 | | | Cote d'Ivoire |
| Douala | 0.0300 | 0.0324 | 3 | 0.1560 | 0.1560 | Cameroon |
| Brazzaville | 0.0124 | 0.0217 | 2 | 0.1897 | 0.1923 | Congo (Dem. Rep.) |
| Kinshasa | 0.0074 | 0.0181 | 12 | 0.1667 | 0.1679 | Congo |
| Djibouti | 0.0128 | 0.0229 | 18 | 0.1817 | 0.1819 | Djibouti |
| Asmara | 0.0205 | 0.0247 | 0 | | | Eritrea |
| Addisabbeba | 0.0217 | 0.0221 | 1 | 0.0627 | 0.0627 | Ethiopia |
| Libreville | 0.0227 | 0.0248 | 4 | 0.1771 | 0.1771 | Gabon |
| Accra | 0.0138 | 0.0182 | 4 | 0.1700 | 0.1718 | Ghana |
| Conakry | 0.0300 | 0.0314 | 0 | | | Guinea |
| Banjul | 0.0217 | 0.0284 | 18 | 0.1688 | 0.1694 | Gambia |
| Bissau | 0.0268 | 0.0273 | 2 | 0.1212 | 0.1212 | Guinea-Bissau |
| Nairobi | 0.0154 | 0.0154 | 0 | | | Kenya |
| Maseru | 0.0194 | 0.0213 | 12 | 0.1517 | 0.1525 | Lesotho |
| Antananarivo | 0.0390 | 0.0409 | 0 | | | Madagascar |
| Bamako | 0.0288 | 0.0309 | 5 | 0.1569 | 0.1569 | Mali |
| Maputo | 0.0167 | 0.0206 | 5 | 0.1526 | 0.1537 | Mozambique |
| Nouakchott | 0.0233 | 0.0303 | 1 | 0.1787 | 0.1787 | Mauritania |
| Blantyre | 0.0294 | 0.0365 | 2 | 0.1928 | 0.1925 | Malawi |
| Windhoek | 0.0341 | 0.0475 | 11 | 0.1870 | 0.1876 | Namibia |
| Niamey | 0.0130 | 0.0198 | 14 | 0.1735 | 0.1744 | Niger |
| Lagos | 0.0188 | 0.0181 | 5 | 0.1767 | 0.1767 | Nigeria |
| Kigali | 0.0175 | 0.0244 | 65 | 0.1643 | 0.1655 | Rwanda |
| Alkhartum | 0.0212 | 0.0218 | 1 | 0.1366 | 0.1366 | Sudan |
| Dakar | 0.0213 | 0.0329 | 11 | 0.1765 | 0.1776 | Senegal |
| Freetown | 0.0270 | 0.0270 | 0 | | | Sierra Leone |
| Mogadishu | 0.0635 | 0.0635 | 0 | | | Somalia |
| Mbabane | 0.0100 | 0.0186 | 209 | 0.1700 | 0.1715 | Swaziland |
| Ndjamena | 0.0210 | 0.0317 | 20 | 0.1873 | 0.1879 | Chad |
| Sokode | 0.0288 | 0.0303 | 5 | 0.1393 | 0.1393 | Togo |
| Daressalaam | 0.0231 | 0.0245 | 17 | 0.1618 | 0.1618 | Tanzania |
| Kampala | 0.0200 | 0.0228 | 2 | 0.1429 | 0.1429 | Uganda |
| Johannesburg | 0.0318 | 0.0367 | 4 | 0.1528 | 0.1528 | South Africa |
| Lusaka | 0.0185 | 0.0293 | 19 | 0.1769 | 0.1776 | Zambia |
| Harare | 0.0011 | 0.0014 | 19 | 0.1403 | 0.1403 | Zimbabwe |

*Notes*: The table reports summary statistics for the primary city and secondary cities in each country. The annualized growth rates are based on average light intensity and computed as $\frac{1}{21}(\ln x_{2013} - \ln x_{1992})$. The growth rate of secondary cities is an average across all such cities in the country.

**Table J-3** – Growth regressions varying the minimum secondary city size, intensive margin

| | *Dependent variable: Log lights in the initial footprint* | | | | | | | |
|---|---|---|---|---|---|---|---|---|
| | Stable lights | Corrected | Stable lights | Corrected | Stable lights | Corrected | Stable lights | Corrected |
| | (1) | (2) | (3) | (4) | (5) | (6) | (7) | (8) |
| Primate × trend | -0.217 | 0.351 | -0.064 | 0.514** | 0.294 | 0.895*** | 0.018 | 0.658*** |
| | (0.267) | (0.234) | (0.266) | (0.228)** | (0.275) | (0.249)*** | (0.238) | (0.209)*** |
| | [0.269] | [0.233] | [0.269] | [0.228]** | [0.272] | [0.242]*** | [0.225] | [0.193]*** |
| Minimum size (in km$^2$) | 6 | 6 | 9 | 9 | 15 | 15 | 25 | 25 |
| City FE | ✓ | ✓ | ✓ | ✓ | ✓ | ✓ | ✓ | ✓ |
| Country-Year FE | ✓ | ✓ | ✓ | ✓ | ✓ | ✓ | ✓ | ✓ |
| Observations | 14916 | 14916 | 12364 | 12364 | 8734 | 8734 | 5962 | 5962 |
| Cities | 678 | 678 | 562 | 562 | 397 | 397 | 271 | 271 |

*Notes*: The table reports the results of city-level panel regressions using the stable lights and top-coding corrected data with varying minimum size thresholds for secondary cities. All coefficients are scaled by 100 for readability. The specifications are variants of $\ln \text{LIGHTS}_{ijt} = \beta_1 t + \beta_2 (t \times P_{ij}) + c_{ij} + s_{jt} + \epsilon_{ijt}$ where $t$ is a linear time trend, $P_{ij}$ is an indicator for primate cities, $c_{ij}$ is a city fixed effect and $s_{jt}$ contains country-year fixed effects. Standard errors clustered at the city level are reported in parentheses. Conley errors with a spatial cutoff of 1,000 km and a time-series HAC with a lag cutoff of 1,000 years are reported in brackets. Significant at: * $p < 0.10$, ** $p < 0.05$, *** $p < 0.01$.

**Table J-4** – Growth regressions excluding major regions, intensive margin

| | *Dependent variable: Log lights in the initial footprint* | | | | | | | |
|---|---|---|---|---|---|---|---|---|
| | Stable lights (1) | Corrected (2) | Stable lights (3) | Corrected (4) | Stable lights (5) | Corrected (6) | Stable lights (7) | Corrected (8) |
| Primate × trend | 0.110 | 0.724 | 0.141 | 0.568 | -0.599 | 0.114 | -0.080 | 0.515 |
| | (0.356) | (0.297)** | (0.274) | (0.249)** | (0.248)** | (0.203) | (0.306) | (0.262)* |
| | [0.355] | [0.293]** | [0.278] | [0.251]** | [0.256]** | [0.205] | [0.301] | [0.256]** |
| Excluded region | West Africa | | Middle Africa | | East Africa | | Southern Africa | |
| City FE | ✓ | ✓ | ✓ | ✓ | ✓ | ✓ | ✓ | ✓ |
| Country-Year FE | ✓ | ✓ | ✓ | ✓ | ✓ | ✓ | ✓ | ✓ |
| Observations | 9240 | 9240 | 11528 | 11528 | 9900 | 9900 | 7018 | 7018 |
| Cities | 420 | 420 | 524 | 524 | 450 | 450 | 319 | 319 |

*Notes*: The table reports the results of city-level panel regressions using the stable lights and top-coding corrected data omitting major regions of Sub-Saharan Africa. All coefficients are scaled by 100 for readability. The specifications are variants of $\ln \text{LIGHTS}_{ijt} = \beta_1 t + \beta_2 (t \times P_{ij}) + c_{ij} + s_{jt} + \epsilon_{ijt}$ where $t$ is a linear time trend, $P_{ij}$ is an indicator for primate cities, $c_{ij}$ is a city fixed effect and $s_{jt}$ contains country-year fixed effects. Standard errors clustered at the city level are reported in parentheses. Conley errors with a spatial cutoff of 1,000 km and a time-series HAC with a lag cutoff of 1,000 years are reported in brackets. Significant at: * $p < 0.10$, ** $p < 0.05$, *** $p < 0.01$.

## J.2 City structure in Africa

In this section, we conduct an exploratory study of how the internal structure of cities is changing over time. Our aim is to show that nighttime lights can be used to better understand whether neighborhoods within African cities are becoming better connected or whether they increasingly resemble loose clusters of disconnected informal settlements. For this part of the analysis, we focus on the "envelope" of the city, that is, the maximum urban extent observed in both the initial and final boundaries. Focusing on the maximum urban extent allows cities to sprawl and become less connected over time (Harari, 2020), while cities in which slums are replaced with formal housing can increase in density and compactness.[6]

We compute two proxies for the variation of urban population density or within-city fragmentation, both of which are known from the literature on urban forms (e.g. see Tsai, 2005). Our first measure is the coefficient of variation of lights per km$^2$, a simple inequality measure capturing the variation of light intensities across an entire city. It is defined as the ratio of the standard deviation to the mean. A high (low) value indicates large (small) within-city differences in the dispersion of light. The index is not bounded from above.

Our second measure of fragmentation is Moran's $I$ (Moran, 1950). Moran's $I$ takes the precise location of each pixel within a city into account and indicates whether similar light intensities cluster together in space. It is defined as

$$I = \frac{N}{S_0} \frac{\sum_i \sum_j w_{ij}(x_i - \bar{x})(x_j - \bar{x})}{\sum_i (x_i - \bar{x})^2}$$

where $N$ is the number of pixels in the initial footprint of the city, $w_{ij}$ are elements of an $N \times N$ inverse distance weight matrix, $S_0$ is the sum of all $w_{ij}$, $x_i$ or $x_j$ is the pixel-level light intensity, and $\bar{x}$ is mean luminosity.[7]

Positive values of Moran's $I$ indicate that pixels are surrounded by others of similar luminosity or population density (positive autocorrelation), while negative values reflect a checkerboard pattern (negative autocorrelation). The index ranges from minus one to one. Light intensities within cities are positively spatially correlated but there is a clear ranking. The index continuously falls as we move from monocentric cities over polycentric cities to decentralized urban sprawl. A monocentric city in which luminosity slowly and gradually decreases from the densely populated center to the sparsely populated outskirts will have a higher Moran's $I$ than a checkered city in which dense and sparsely populated

[6] We still focus on agglomerations which are now defined as all sub-cities which will eventually merge into a single metropolitan area. All results presented here are robust to using the initial footprint only.

[7] We work with a scaled version of Moran's $I$ to make cities consisting of different numbers of pixels comparable, that is, we subtract its expected value under the null hypothesis of no spatial correlation: $I^* = I - \mathbb{E}[I] = I - (-1/(N-1))$.

areas take turns. We scale both indices by 100 for a better exposition.

Panel (a) of Figure J-3 illustrates the heterogeneity of urban structures on the subcontinent and shows that our light-based measures capture meaningful variation. Consider, for example, cities with a high Moran's $I$ and relatively low coefficients of variation, such as Conakry, Dakar, and Cotounou. This combination indicates a regular structure with a bright center surrounded by similarly bright areas with a slow decay towards darker outskirts. Other cities with the same coefficient of variation have a much lower Moran's $I$. Their spatial distribution is considerably more fragmented, matching other accounts. A large part of Abidjan's population, for example, lives in slums characterized by illegal land tenure, buildings made out of non-permanent materials, and little or next to no infrastructure (UN-Habitat, 2003).

Johannesburg is an interesting case in terms of fragmentation. In 2000, it has one of the highest coefficients of variation and the lowest Moran's $I$ in our sample of primate cities. Owing to a legacy of racial segregation during Apartheid, Johannesburg consists of alternating poor and rich neighborhoods which do not form a single integrated city. There is some limited evidence that this pattern may be changing. Panel (b) of Figure J-3 shows that we observe a moderate increase in Moran's $I$ since the mid-2000s. The coefficient of variation is decreasing at the same time. This suggests that the different neighborhoods could be integrating, although the overall levels of inequality and fragmentation remain very high when compared with other cities in our sample.[8] Just as before, these raw time trends are only suggestive, as they include substantial measurement error.

We use the same methods to analyze these data in a more structured manner and focus on the differential between city types—i.e., we regress one of the measures of city fragmentation, $F_{ijt}$, on a linear time trend, an interaction of a linear time trend with an indicator for primate cities, $P_{ij}$, the log of lights per km$^2$ in the city, $\ln \textsc{Lights}_{ijt}$, and a set of fixed effects. We include the city-wide average light intensity to analyze their changing structure net of scale effects.

Table J-5 suggests two stylized patterns. First, we observe a decrease in the dispersion of lights over time which differs strongly across the two city types. Panel A shows that the coefficient of variation has been decreasing steadily over the period from 1992 to 2013. All three data sources agree on this trend. Panel B analyzes the development of Moran's $I$ as a measure of spatial autocorrelation. The results suggest that there is no robust difference between primary and secondary cities using the corrected or radiance-calibrated data.

Table J-6 provides some preliminary evidence on whether urban form has an effect on city growth. To study this question, we regress log mean lights on the coefficient of variation or Moran's $I$ in the previous year, a linear time trend, an interaction with primacy, and a combination of city and city-year fixed effects. Greater spatial inequality

[8]The evidence is stronger if we focus on the initial footprint and ignore that Johannesburg is sprawling. The rise towards the end of the sample is steeper and exceeds the values of the 1990s.

appears to have a robust negative effect on growth, but the impact of clustering is small and not robust. City structure and growth are endogenous, so that we only consider this an interesting partial correlation which could be explored in future research.

Our preferred interpretation of these findings is that Africa's biggest cities are at a crossroads. They are growing rapidly at the intensive and extensive margin, while the distribution of economic activity and people is starting to equalize across the city. Whether this conclusively demonstrates that poorer neighborhoods are becoming denser and brighter relative to the center but remain disconnected to other neighborhoods remains an open question. Further research might consider combining our corrected lights data with population grids and data on infrastructure to derive policy implications. Researchers interested in analyzing the structure of cities using the DMSP nighttime lights should also take the inherent auto-correlation in the data generating process into account (also see Abrahams et al., 2018, Gibson et al., 2021).

**Figure J-3** – Varying structures of cities in Sub-Saharan Africa

**(a)** Fragmentation in primate cities, 2000 **(b)** Moran's $I$ in Johannesburg

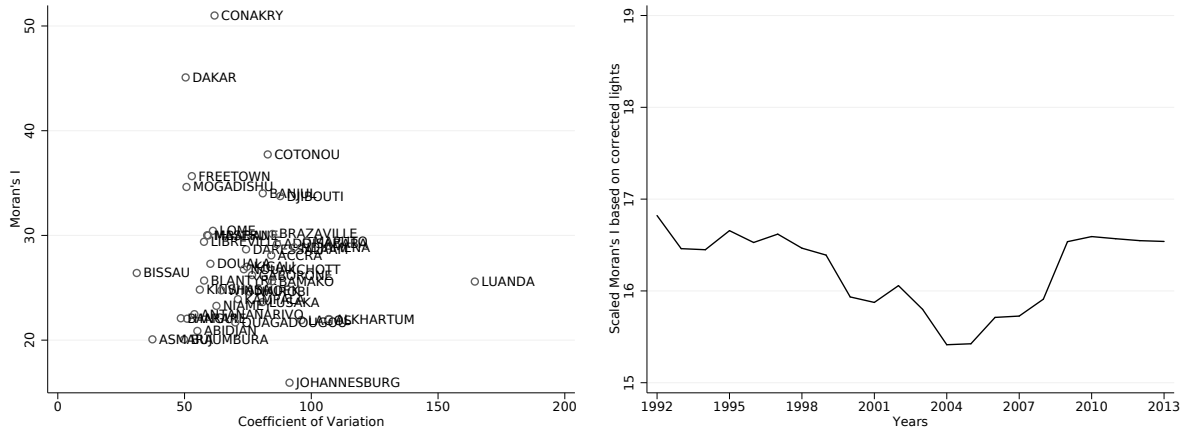


*Notes*: The figure illustrates urban structures in Sub-Saharan Africa. Panel (a) shows a cross-sectional scatter plot of the estimated coefficient of variation (CV) and Moran's $I$ in 2000. Panel (b) displays the evolution of Moran's $I$ in Johannesburg over the period from 1992 to 2013.

**Table J-5** – Trends in fragmentation for African cities, envelopes

| | *Dependent variable: Varies by panel* | | | | | |
|---|---|---|---|---|---|---|
| | *Stable lights* | | *Corrected lights* | | *Radcal lights* | |
| | (1) | (2) | (3) | (4) | (5) | (6) |
| | *Panel a) Coefficient of variation in the envelope* | | | | | |
| Primate × trend | -1.095 | -1.048 | -0.797 | -0.657 | -0.935 | -0.992 |
| | (0.146)*** | (0.148)*** | (0.128)*** | (0.146)*** | (0.217)*** | (0.257)*** |
| | [0.150]*** | [0.146]*** | [0.133]*** | [0.145]*** | [0.215]*** | [0.252]*** |
| Lights per km$^2$ | -19.477 | -17.411 | -18.732 | -17.334 | -5.630 | -1.699 |
| | (1.935)*** | (1.978)*** | (1.871)*** | (1.997)*** | (4.267) | (3.388) |
| | [2.096]*** | [2.192]*** | [2.028]*** | [2.184]*** | [4.349] | [3.776] |
| Observations | 12356 | 12356 | 12356 | 12356 | 3932 | 3932 |
| Cities | 562 | 562 | 562 | 562 | 562 | 562 |
| | *Panel b) Moran's I in the envelope* | | | | | |
| Primate × trend | -0.063 | -0.051 | -0.020 | 0.004 | -0.092 | -0.018 |
| | (0.029)** | (0.040) | (0.027) | (0.036) | (0.052)* | (0.059) |
| | [0.030]** | [0.039] | [0.029] | [0.035] | [0.057] | [0.057] |
| Lights per km$^2$ | -1.191 | -1.296 | -1.232** | -1.456** | -0.902 | -1.169 |
| | (0.501)** | (0.618)** | (0.496)** | (0.617)** | (0.574) | (0.715) |
| | [0.509]** | [0.604]** | [0.504]** | [0.604]** | [0.585] | [0.691] |
| Observations | 12356 | 12356 | 12356 | 12356 | 3932 | 3932 |
| Cities | 562 | 562 | 562 | 562 | 562 | 562 |
| City FE | ✓ | ✓ | ✓ | ✓ | ✓ | ✓ |
| Year FE | ✓ | – | ✓ | – | ✓ | – |
| Country-Year FE | – | ✓ | – | ✓ | – | ✓ |

*Notes*: The table reports results of city-level panel regressions using the stable lights, top-coding corrected data, as well as the radiance-calibrated data. The specifications are variants of $F_{ijt} = \beta_1 t + \beta_2(t \times P_{ij}) + \beta_3 \ln \textsc{Lights}_{ijt} + c_{ij} + s_{jt} + \epsilon_{ijt}$, where $F_{ijt}$ is either the coefficient of variation (Panel A) or Moran's $I$ (Panel B), $t$ is a linear time trend, $P_{ij}$ is an indicator for primate cities, $c_{ij}$ is a city fixed effect and $s_{jt}$ contains are varying set of fixed effects (year, or country-year). Standard errors clustered at the city level are reported in parentheses. Conley errors with a spatial cutoff of 1,000 km and a time-series HAC with a lag cutoff of 1,000 years are reported in brackets. Significant at: * $p < 0.10$, ** $p < 0.05$, *** $p < 0.01$.

**Table J-6** – Impact of fragmentation on city growth, envelopes

| | *Dependent variable: Log lights in the envelope* | | | | | |
|---|---|---|---|---|---|---|
| | *Stable lights* | | *Corrected lights* | | *Radcal lights* | |
| | (1) | (2) | (3) | (4) | (5) | (6) |
| | *Panel a) Impact of coefficient of variation on growth* | | | | | |
| Primate × trend | 0.003 | 0.001 | 0.007 | 0.006 | 0.029 | 0.032 |
| | (0.002) | (0.002) | (0.003)** | (0.002)*** | (0.008)*** | (0.006)*** |
| | [0.003] | [0.003] | [0.003]** | [0.002]*** | [0.008]*** | [0.005]*** |
| Lagged CV | -0.006 | -0.004 | -0.006 | -0.004 | -0.003 | -0.003 |
| | (0.001)*** | (0.001)*** | (0.001)*** | (0.001)*** | (0.001)*** | (0.001)*** |
| | [0.001]*** | [0.001]*** | [0.001]*** | [0.001]*** | [0.001]*** | [0.001]*** |
| Observations | 11791 | 11791 | 11791 | 11791 | 1120 | 1122 |
| Cities | 562 | 562 | 562 | 562 | 560 | 562 |
| | *Panel b) Impact of Moran's I on growth* | | | | | |
| Primate × trend | 0.010 | 0.005 | 0.013 | 0.009 | 0.033 | 0.035 |
| | (0.003)*** | (0.003)** | (0.004)*** | (0.002)*** | (0.008)*** | (0.006)*** |
| | [0.003]*** | [0.003]** | [0.004]*** | [0.002]*** | [0.008]*** | [0.006]*** |
| Lagged Moran's I | -0.003 | -0.002 | -0.003 | -0.002 | -0.002 | -0.000 |
| | (0.002) | (0.002) | (0.002) | (0.002) | (0.003) | (0.003) |
| | [0.002] | [0.002] | [0.002] | [0.002] | [0.003] | [0.003] |
| Observations | 11791 | 11791 | 11791 | 11791 | 1120 | 1122 |
| Cities | 562 | 562 | 562 | 562 | 560 | 562 |
| City FE | ✓ | ✓ | ✓ | ✓ | ✓ | ✓ |
| Year FE | ✓ | – | ✓ | – | ✓ | – |
| Country-Year FE | – | ✓ | – | ✓ | – | ✓ |

*Notes*: The table reports the results of city-level panel regressions using the stable lights, top-coding corrected data, as well as the radiance-calibrated lights, where either the lagged coefficient of variation or Moran's $I$ are used as regressors ($F_{ij,t-1}$). All coefficients are scaled by 100 for readability. The specifications are variants of $\ln \text{LIGHTS}_{ijt} = \beta_1 t + \beta_2(t \times P_{ij}) + \beta_3 F_{ij,t-1} + c_{ij} + s_{jt} + \epsilon_{ijt}$ where $t$ is a linear time trend, $P_{ij}$ is an indicator for primate cities, $c_{ij}$ is a city fixed effect and $s_{jt}$ contains a varying set of fixed effects (year, or country-year). Standard errors clustered at the city level are reported in parentheses. Conley errors with a spatial cutoff of 1,000 km and a time-series HAC with a lag cutoff of 1,000 years are reported in brackets. Significant at: * $p < 0.10$, ** $p < 0.05$, *** $p < 0.01$.

# Additional references


Abrahams, A., C. Oram, and N. Lozano-Gracia (2018). Deblurring DMSP nighttime lights: A new method using gaussian filters and frequencies of illumination. *Remote Sensing of Environment 210*, 242–258.

Bruederle, A. and R. Hodler (2018, 09). Nighttime lights as a proxy for human development at the local level. *PLOS ONE 13*(9), 1–22.

Chen, X. and W. D. Nordhaus (2011). Using luminosity data as a proxy for economic statistics. *Proceedings of the National Academy of Sciences 108*(21), 8589–8594.

Cirillo, P. (2013). Are your data really Pareto distributed? *Physica A: Statistical Mechanics and its Applications 392*(23), 5947–5962.

Coles, S. (2001). *An introduction to the statistical modeling of extreme values*. Springer Series in Statistics.

Eeckhout, J. (2009). Gibrat's law for (all) cities: Reply. *American Economic Review 99*(4), 1676–1683.

Elvidge, C. D., K. E. Baugh, J. B. Dietz, T. Bland, P. C. Sutton, and H. W. Kroehl (1999). Radiance calibration of DMSP-OLS low-light imaging data of human settlements. *Remote Sensing of Environment 68*(1), 77–88.

Elvidge, C. D., F.-C. Hsu, K. E. Baugh, and T. Ghosh (2014). National trends in satellite-observed lighting. In Q. Weng (Ed.), *Global Urban Monitoring and Assessment through Earth Observation*, Taylor & Francis Series in Remote Sensing Applications, Chapter 6, pp. 97–119. CRC Press.

Elvidge, C. D., D. Ziskin, K. E. Baugh, B. T. Tuttle, T. Ghosh, D. W. Pack, E. H. Erwin, and M. Zhizhin (2009). A fifteen year record of global natural gas flaring derived from satellite data. *Energies 2*(3), 595–622.

Gabaix, X. (2009). Power laws in economics and finance. *Annual Review of Economics 1*(1), 255–294.

Gabaix, X. and R. Ibragimov (2011). Rank - 1/2: A simple way to improve the OLS estimation of tail exponents. *Journal of Business & Economic Statistics 29*(1), 24–39.

Gabaix, X. and Y. Ioannides (2004). The evolution of city size distribution. In J. V. Henderson and J. F. Thisse (Eds.), *Handbook of Regional and Urban Economics* (1 ed.), Volume 4, Chapter 53, pp. 2341–2378. Elsevier.

Gibson, J., S. Olivia, and G. Boe-Gibson (2021). Which night lights data should we use in economics, and where? *Journal of Development Economics 149*, 102602.

Harari, M. (2020). Cities in bad shape: Urban geometry in India. *American Economic Review 110*(8), 2377–2421.

Henderson, J. V., A. Storeygard, and D. N. Weil (2012). Measuring economic growth from outer space. *American Economic Review 102*(2), 994–1028.

Hill, B. (1975). A simple general approach to inference about the tail of a distribution. *The Annals of Statistics 3*(5), 1163–1174.

Hsu, F.-C., K. E. Baugh, T. Ghosh, M. Zhizhin, and C. D. Elvidge (2015). DMSP-OLS radiance calibrated nighttime lights time series with intercalibration. *Remote Sensing 7*(2), 1855–1876.

Hu, Y. and J. Yao (2019). Illuminating economic growth. IMF Working Paper no. 19/77, International Monetary Fund.

Michalopoulos, S. and E. Papaioannou (2013). Pre-colonial ethnic institutions and contemporary African development. *Econometrica 81*(1), 113–152.

Mookherjee, D. and A. Shorrocks (1982). A decomposition analysis of the trend in UK income inequality. *Economic Journal 92*(368), 886–902.

Moran, A. P. (1950). Notes on continuous stochastic phenomena. *Biometrika 37*(1/2), 17–23.

Newman, M. (2005). Power laws, Pareto distributions and Zipf's law. *Contemporary Physics 46*(5), 323–351.

Nordhaus, W. and X. Chen (2015). A sharper image? Estimates of the precision of nighttime lights as a proxy for economic statistics. *Journal of Economic Geography 15*(1), 217–246.

Tsai, Y.-H. (2005). Quantifying urban form: Compactness versus 'sprawl'. *Urban Studies 42*(1), 141–161.

Tuttle, B., S. Anderson, P. Sutton, C. Elvidge, and K. Baugh (2013). It used to be dark here. *Photogrammetric Engineering and Remote Sensing 79*(3), 287–297.

UN-Habitat (2003). *The challenge of slums: Global report on human settlements, 2003*. Earthscan Publications.

Ziskin, D., K. Baugh, F. C. Hsu, T. Ghosh, and C. Elvidge (2010). Methods used for the 2006 radiance lights. *Proceedings of the Asia-Pacific Advanced Network 30*, 131–142.